TEXTURE SEGREGATION, SURFACE REPRESENTATION, AND FIGURE-GROUND SEPARATION

Stephen Grossberg†

Department of Cognitive and Neural Systems
and
Center for Adaptive Systems
Boston University
677 Beacon Street
Boston, Massachusetts 02215 §

and

Luiz Pessoa‡

Department of Computer and Systems Engineering
Federal University do Rio de Janeiro
Rio de Janeiro, Brazil

Running head: Texture segregation and figure-ground separation

---

Abstract

A widespread view is that most of texture segregation can be accounted for by differences in the spatial frequency content of texture regions. Evidence from both psychophysical and physiological studies indicate, however, that beyond these early filtering stages, there are stages of 3-D boundary segmentation and surface representation that are used to segregate textures. *Chromatic* segregation of element-arrangement patterns – as studied by Beck and colleagues – cannot be completely explained by the filtering mechanisms previously employed to account for *achromatic* segregation. An element arrangement pattern is composed of two types of elements that are arranged differently in different image regions (e.g., vertically on top and diagonally on bottom). FACADE theory mechanisms that have previously been used to explain data about 3-D vision and figure-ground separation are here used to simulate chromatic texture segregation data, including data with equiluminant elements on dark or light homogenous backgrounds, or backgrounds composed of vertical and horizontal dark or light stripes, or horizontal notched stripes. These data include the fact that segregation of patterns composed of red and blue squares decreases with increasing luminance of the interspaces. Asymmetric segregation properties under 3-D viewing conditions with the equiluminant elements close or far are also simulated. Two key model properties are a spatial impenetrability property that inhibits boundary grouping across regions with noncolinear texture elements, and a boundary-surface consistency property that uses feedback between boundary and surface representations to eliminate spurious boundary groupings and separate figures from their backgrounds.

Key words: figure-ground, perception, texture segregation, 3-D vision, grouping, boundary, surface, color vision, neural networks, filling-in

1   Introduction

A widespread view is that most of texture segregation can be accounted for by differences in the spatial frequency content of texture regions, and several research groups have proposed theoretical models of this kind to account for experimental results (Bergen and Landy, 1991; Daugman, 1988; Graham, Beck and Sutter, 1992; Malik and Perona, 1990; Sutter, Beck, and Graham, 1989). This hypothesis is often cast in terms of oriented spatial frequency selective operators thought to resemble mechanisms existing at relatively low levels in the visual system; e.g., cortical simple cells. Despite the relative success of the spatial frequency hypothesis, it is inadequate as a general account of image segmentation. Evidence from both psychophysical and neurophysiological studies indicate that, beyond this early multiple-scale filtering stage, there are stages of context-sensitive grouping (Beck *et al.*, 1983; Gregory and Heard, 1979; Kanizsa, 1979; Kawabata, 1984; Petry and Meyer, 1987; von der Heydt *et al.*, 1984) and 3-D surface representation (Gibson, 1950; He and Nakayama, 1994; Kanizsa, 1979; Nakayama and Shimojo, 1990). The present article describes a model that incorporates multiple-scale filters, context-sensitive grouping, and 3-D surface representation, and uses it to simulate texture percepts that cannot be explained by filtering alone.

   Grossberg and Mingolla (1985a, 1985b, 1987) introduced a monocular version of this model and used it to explain data about form and color perception, including texture segregation. This model includes both multiple-scale filters and context-sensitive grouping, or segmentation, mechanisms. Variants of this multiple-scale filter were used to simulate texture segregation in the above cited articles; e.g., Sutter *et al.* (1989). The Grossberg-Mingolla model was later extended to study 3-D vision and figure-ground perception, including 3-D surface representation (Grossberg, 1987a, 1994, 1995). This extended model has been called FACADE theory, since it attempts to explain how the brain generates representations of **F**orm-**A**nd-**C**olor-**A**nd **DE**pth.

   Within FACADE theory, early filtering mechanisms activate the formation of 3-D boundary groupings, which, in turn, organize the selective filling-in of 3-D surface representations. These boundaries and surfaces are formed according to different, indeed, complementary, computational rules (Grossberg, 1987a; Grossberg, Mingolla, and Todorović, 1989). They arrive at a mutually consistent representation through reciprocal interactions. These interactions have been interpreted in terms of pathways joining the interblob and blob cortical streams between cortical areas V1 to V4 (Grossberg, 1994a). They are here used to explain texture segregation data for which early filtering mechanisms are insufficient.

   Our analysis focuses upon a challenging family of texture images that Beck and colleagues have called element-arrangement patterns (Beck *et al.*, 1991; Beck *et al.*, 1987; Graham *et al.*, 1992; Sutter *et al.*, 1989). These patterns were designed to probe key properties of texture segregation in a parametrically controllable fashion. An element-arrangement pattern is composed of two types of elements that differ in the ways in which they are arranged in different regions of the pattern. Figure 1A illustrates an element-arrangement pattern in which the elements are filled and unfilled squares arranged in a striped pattern in the top region and in a checkerboard pattern in the bottom region. Beck *et al.* (1987) suggested that the perceived segregation of achromatic element-arrangement
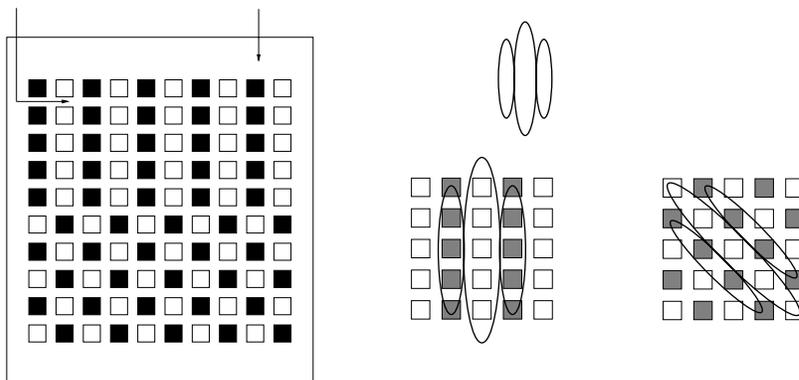
Figure 1: (A) An illustration of an element-arrangement pattern composed of filled and unfilled squares. Arrows indicate the surround (the space surrounding a pattern) and the interspace (the spaces between the squares) regions. (B) An illustration of how responses of cells with oriented receptive fields may account for element-arrangement segregation. Top: Excitatory and inhibitory lobes of an even symmetric operator. Bottom. Left: Large vertical receptive fields respond strongly to the vertical columns of squares in the striped region. Right: Large oblique receptive fields respond strongly to the diagonal columns of squares in the checkerboard region.

patterns was qualitatively consistent with the hypothesis that differences in the outputs of spatial frequency channels were sufficient to explain the perceived segregation; higher-order processes of grouping and surface representation were not essential. They proposed that the differential responses of oriented simple cell-like mechanisms to the striped and checked regions of an element-arrangement pattern is the basis for the perceived segregation (Figure 1B). Sutter *et al.* (1989) provided further support for this hypothesis by showing that the perceived segregation of patterns composed of large and small squares was minimal when the area × contrast of the squares was equal. The area × contrast of the large and small squares is the same when the greater area of the large square is compensated for by the higher contrast of the small square. Squares that have the same area × contrast produce the same output at the fundamental frequency of the pattern; that is, the frequency which, when the excitatory region of a receptive field falls on one column of squares, the inhibitory region of the receptive field falls on the adjacent column of squares (see Figure 1B).

Beck (1994) and Pessoa, Beck, and Mingolla (1996) have recently investigated element-arrangement segregation with chromatic patterns. Beck *et al.* (1987) originally showed that chromatic differences alone support perceived segregation by obtaining strong segregation in element-arrangement patterns composed of equal luminance squares on an equal-luminance background (see also Pessoa *et al.*, 1996). Beck (1994) showed, in addition, that the strength of segregation of patterns composed of red and blue patterns, rather than achromatic patterns such as in Figure 1B, is inversely proportional to the luminance

of the interspaces, such that the greater the luminance the weaker the segregation.

The present paper describes how FACADE theory can explain the findings on chromatic segregation of element-arrangement patterns. In particular, it will be shown how the results arise from circuits previously employed to account for 3-D vision and figure-ground separation using, as a front end, filtering and segmentation mechanisms that have previously been used to simulate data on grouping processes in texture segregation (Grossberg, 1987a; Grossberg and Mingolla, 1985a, 1985b, 1987).

1.1   Asymmetries in Chromatic Texture Segregation

In order to describe how FACADE theory can explain chromatic element-arrangement segregation, we will concentrate on a few key experimental findings that pose the greatest theoretical challenge, since they reveal *asymmetries* in texture segregation. At the same time, they serve to illustrate the main FACADE mechanisms of figure-ground separation needed to account for the results, while highlighting the insufficiency of filtering schemes alone. The cases we discuss are illustrated in Figure 2.

First, segregation is strong on a black background and weak on a white background (Figure 2A [top row]). Pessoa *et al.* (1996) showed that the ratio of interspace to square luminance determines segregation—not absolute luminance—but that direction of contrast, or polarity, is important. Mechanisms involving full-wave rectifying or squaring nonlinearities respond as in Sutter *et al.* (1989) to amount of contrast but are insensitive to direction of contrast.

Second, Beck (1994) showed that horizontal interspaces interfere with segregation more than vertical interspaces; see Figure 2A (row 2) for examples. In other words, the geometrical arrangement of the interspaces had a significant effect on perceived segregation. Beck (1994) interpreted his results in terms of grouping mechanisms that are more severely affected by horizontal interspaces because they are orthogonal to the vertical arrangement of the squares on the top region of the displays. Although more sophisticated filtering schemes may be able to account for this asymmetry, simple schemes cannot readily account for it.

Beck (1994) also showed that segregation is inversely proportional to interspace luminance. As the luminance of the entire background, or the luminance of the vertical or horizontal interspaces, is increased, segregation strength decreases. Moreover, perceived segregation decreases more and in a similar manner when either the luminance of the entire interspace or the luminance of the horizontal interspaces is increased than when the luminance of the vertical interspaces is increased (see Figure 6, left) — accordingly, segregation for vertical interspaces is stronger than for horizontal interspaces.

Third, the introduction of depth (through binocular disparity) does not improve perceived segregation when the squares are seen in front, but improves segregation when horizontal interspaces are seen in front; see Figure 2B (top two rows). Why does the introduction of depth change the information used for texture segregation in one case, but not in the other? The figure-ground mechanisms of FACADE theory clarify how depth reorganizes the percept when horizontal interspaces are seen in front, thereby producing amodal completion of the squares "behind" the lines and strong segregation. When the squares are seen in front, no reorganization takes place on the depth plane "behind", and segregation is largely unaltered. Filtering mechanisms alone cannot account for the improvement in
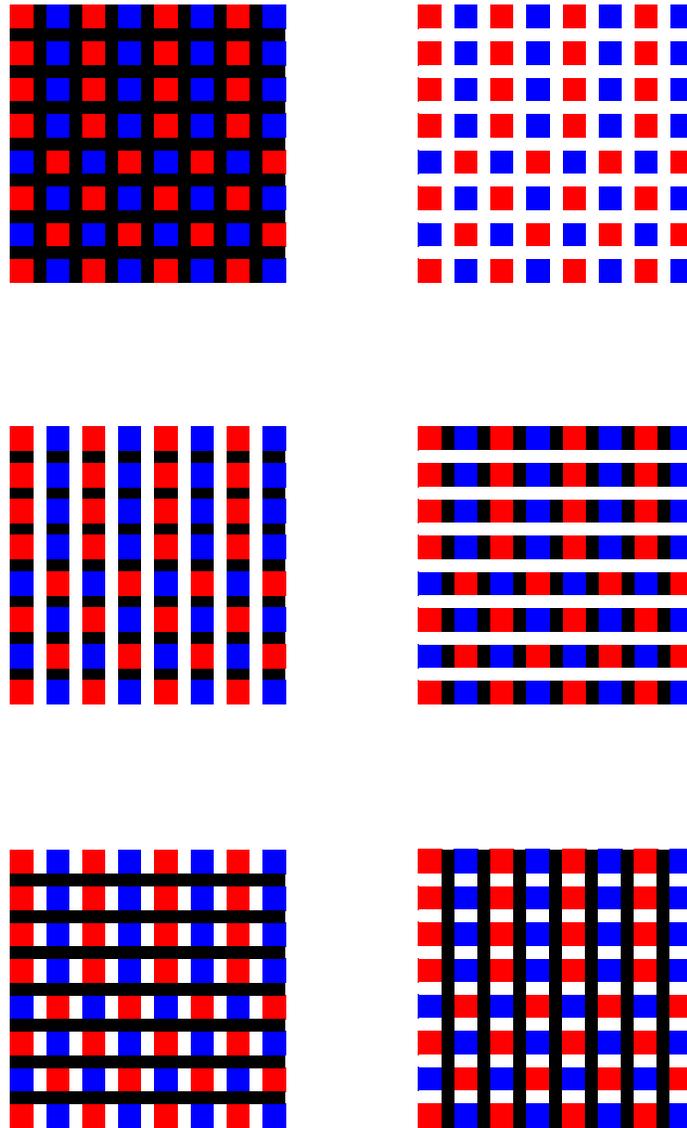
Figure 2: Chromatic element-arrangement patterns. All displays are composed of red and blue squares and achromatic interspaces. Squares are organized vertically in the top of the display and diagonally in the bottom. Displays are intended for illustration of main properties only. (A) Top left: Perceived segregation is strong when background is black. Top right: Segregation is weak when background is white. Middle left: Vertical interspaces are white. Middle right: Horizontal interspaces are white. Perceived segregation is stronger when the vertical interspaces are white than when the horizontal interspaces are white. Bottom left: Vertical segments are white. Bottom right: Horizontal segments are white. Perceived segregation is stronger when the vertical segments are white than when the horizontal segments are white.
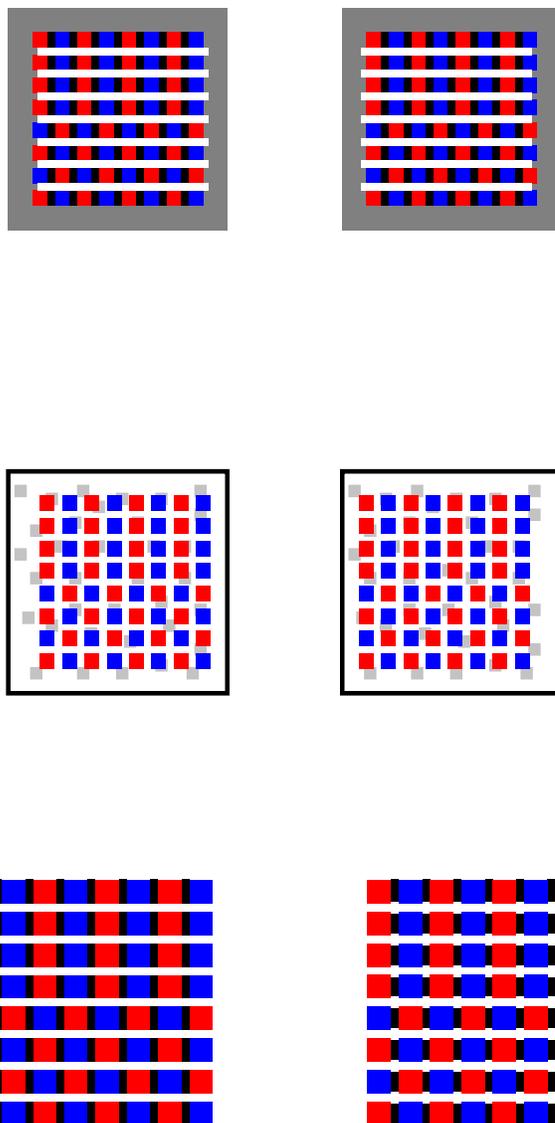
Figure 2: (B) Top: When the left and right stereoimages are fused (by "uncrossing") the horizontal interspaces are seen in front of the red and blue squares. Perceived segregation is greatly improved. Note that the vertically aligned squares in the top half of the display amodally complete in the back. Middle: When the left and right stereoimages are fused (by "uncrossing") the red and blue squares are seen in front of the white background. Perceived segregation is poor. Note that in order to stably perceive the white background in back, a collection of zero disparity gray squares is used so that the background as a whole is "captured" at zero disparity. In actual experiments, smaller low luminance green dots were used (see Pessoa *et al.* (1996) for details). Bottom left: Horizontal interspaces are white. The pop-out of the horizontal white lines is facilitated by having thinner lines relative to the red and blue squares. Under such conditions, perceived segregation is improved. Bottom right: Small vertical segments are added to horizontal white lines. Perceived segregation is poorer than with horizontal white lines alone since pop-out is not favored by the local geometry produced by the introduction of the small vertical segments.

segregation with the introduction of depth for horizontal interspaces, let alone why in one case perceived segregation improves and in the other it does not.

Next we provide a review of the main mechanisms of FACADE theory that will be invoked below. For a comprehensive exposition, see Grossberg (1994). Readers with some knowledge of model concepts can skip directly to the data analysis in Section 3.

2   Review of FACADE Theory

FACADE theory postulates that two complementary systems and their interactions are responsible for producing a unified 3-D percept: the Boundary Contour System (BCS) and the Feature Contour System (FCS). The BCS is responsible for boundary formation, regularization, and completion and provides mechanisms for the grouping and segregation of image regions. The BCS creates an emergent 3-D boundary segmentation that combines scenic information from edges, texture, shading, and stereo information at multiple spatial scales (Grossberg, 1987b, 1994; Grossberg and Marshall, 1989; Grossberg and McLoughlin, 1997; Grossberg and Mingolla, 1985a, 1985b, 1987; Grossberg *et al.*, 1995, 1997; Grossberg and Wyse, 1991; McLoughlin and Grossberg, 1997). The FCS is responsible for 3-D surface representation. It compensates for variable illumination conditions and fills-in surface properties of brightness, color, depth, and form among multiple spatial scales (Arrington, 1994; Cohen and Grossberg, 1984; Grossberg, 1987a, 1987b; Grossberg and Mingolla, 1985a; Grossberg and Todorović, 1988; Grossberg *et al.*, 1995; Paradiso and Nakayama, 1991; Pessoa *et al.*, 1995; Neumann, 1996).

The review of FACADE theory will be given in two stages. First the monocular mechanisms of the BCS and FCS will be described to clarify the basic boundary and surface operations. Then the binocular extension of FACADE theory will be reviewed in order to introduce the processing stages that will be needed to explain the types of percepts surveyed above. The binocular FACADE theory clarifies how signals from multiple receptive field sizes are combined in order to generate 3-D percepts of the world. These summaries will be given in heuristic terms in order to bring out the main ideas. Readers who desire mathematical descriptions with supportive computer simulations of other data can find them in a number of recent articles (Francis and Grossberg, 1996a, 1996b; Francis *et al.*, 1994; Gove *et al.*, 1995; Grossberg and McLoughlin, 1997; Grossberg *et al.*, 1995; Waxman *et al.*, 1995). These simulations collectively demonstrate that the FACADE theory mechanisms discussed herein work as described below. The model that is simulated herein has been simplified both to focus on the most relevant processes and to achieve computational tractability.

2.1   A Monocular BCS Model of Cortical Boundary
    Segmentation

The BCS consists of multiple fields of cells, or copies, each with cells whose receptive fields are sensitive to a different range of image sizes. Each BCS copy consists of a filter followed by a grouping, or boundary completion, network. The BCS models the cortical processing stream that begins in the lateral geniculate nucleus (LGN) and ends in extrastriate cortical
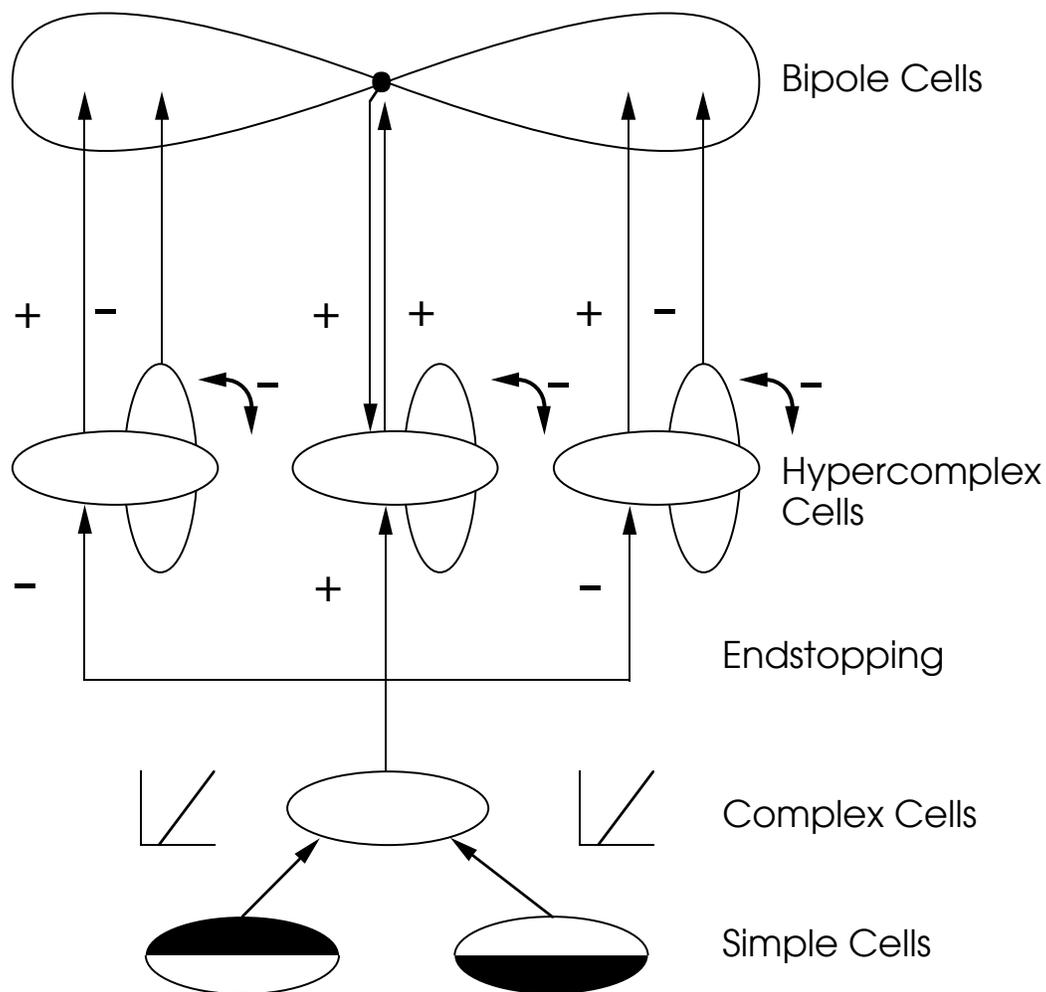
Figure 3: Simple cells compute local oriented contrast. They are sensitive to contrast polarity. Their activities are half-wave rectified to generate output signals. Oppositely polarized simple cell outputs activate complex cells. Complex cells activate spatial and orientational competition among endstopped complex (or hypercomplex) cells. Hypercomplex cells excite bipole cells with similar orientational preference and inhibit bipole cells with (nearly) perpendicular orientational preference. Coactivation of both branches of a bipole cell receptive field generates feedback that initiates the long-range grouping process.

area V4 (DeYoe and van Essen, 1988) after passing through the interblobs of cortical area V1 and the interstripes of cortical area V2.

The model LGN ON and OFF cells receive input from retinal ON and OFF cells. ON cells are turned on by increments in image contrasts, whereas OFF cells are turned off. (See Schiller, 1992 for a review.) Because these ON and OFF cells have antagonistic surrounds and obey membrane, or shunting, equations, they help to discount the illuminant, normalize image activities, and extract ratio contrasts from an image (Grossberg, 1983).

The LGN cell outputs activate the first stage of cortical BCS processing, the simple cells; see Figure 3. Simple cells are oriented local contrast detectors that respond to a prescribed contrast polarity, or direction-of-contrast. Spatially displaced LGN ON and OFF cells input to pairs of like-oriented simple cells that are sensitive to opposite directions-of-contrast. These simple cell pairs compete with each other before generating output signals; cf., Ohzawa *et al.* (1990), Ferster (1988), and Liu *et al.* (1992) for relevant data.

Pairs of simple cells sensitive to like position and orientation but opposite direction-of-contrast generate half-wave rectified output signals that summate at the next processing stage to activate complex cells (Figure 3). The target complex cells are thus sensitive to the same position and orientation as the simple cells, but pool together opposite contrast polarities. The net effect is to perform an oriented full-wave rectification of the image. The rectified output from a complex cell activates a second filter which carries out spatial and orientational competition that converts complex cells into endstopped complex cells, also called hypercomplex cells (Figure 3). Spatial competition realizes an endstopping operation by exciting like-oriented hypercomplex cells at the same position and orientation while inhibiting nearby hypercomplex cells that code similar orientations. Orientational competition occurs in a push-pull fashion between hypercomplex cells at the same position. Maximum inhibition occurs between mutually perpendicular orientations.

Graham *et al.* (1992) have presented a texture segregation model similar to the double-filter model in Figure 3 to explain the segregation of element-arrangement patterns containing balanced elements with no energy at the fundamental frequency. Two key differences (which will be expanded below) play a role in our explanations: Each BCS simple cell filters only one contrast polarity before its total activation is thresholded, half-wave rectified, and pooled across polarity at complex cells. In Graham *et al.* (1992), both polarities are simultaneously pooled at complex cells. The models can thus respond differently to direction-of contrast in a textured scene. In addition, the BCS does not merely pool filter outputs. Rather, it contains cooperative bipole cells (see Figure 3) that can group hypercomplex cell signals in a context-sensitive fashion over a variety of positions and orientations.

Hypercomplex cells interact with bipole cells as part of a grouping network, called the cooperative-competitive (CC) loop, which includes feedback between bipole cells and hypercomplex cells; see Figure 3. Individual bipole cells can fire back towards like-oriented hypercomplex cells if both lobes of the bipole cell receptive field are sufficiently activated. Such activation must fall within a band of orientations that are similar to the receptive fields axis of the bipole cell. Bipole cells hereby behave like statistical AND gates that fire when they detect suitably oriented boundary inducers in both lobes of their receptive field. The existence of bipole cells was predicted (Cohen and Grossberg, 1984; Grossberg, 1984; Grossberg and Mingolla, 1985a, 1985b) shortly before von der Heydt and colleagues reported analogous cells properties in monkey visual area V2 (von der Heydt, Peterhans,

and Baumgartner, 1984). Feedback between the longer-range cooperative bipole cells and shorter-range competitive hypercomplex cells help to select the statistically most favored boundaries while suppressing weaker grouping possibilities. Another relevant point is that (say) a horizontal bipole cell is inhibited by activation of vertical hypercomplex cells (Figure 3) as well as being excited by horizontal hypercomplex cells. This *spatial impenetrability* operation (Grossberg, 1987a; Grossberg and Mingolla, 1987) interferes with colinear grouping across regions wherein non-colinear orientations are present.
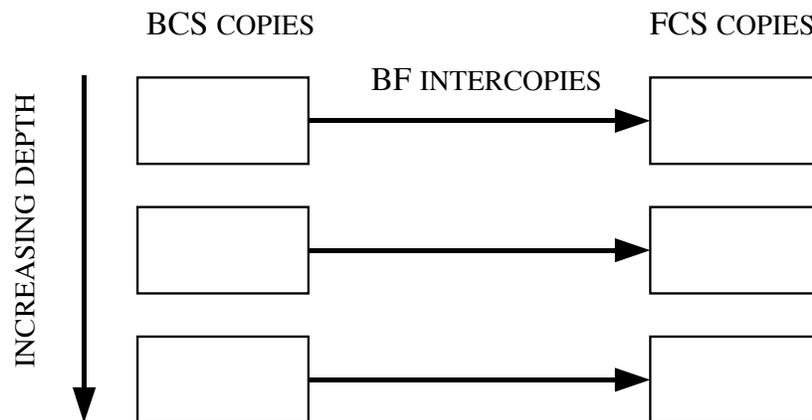
2.2 Filling-In of Monocular Surface Representations within the FCS

The FCS models the cortical processing stream from the LGN to cortical area V4 that passes through the blobs of cortical area V1 and the thin stripes of cortical area V2 (DeYoe and van Essen, 1988). In the monocular BCS model, each BCS boundary segmentation generates topographic output signals to ON and OFF Filling-In DOmains, or FIDOs. These FIDOs also receive inputs from the ON and OFF LGN cells, respectively. The LGN inputs activate their target cells, which allow activation to diffuse rapidly to neighboring FIDO cells. This diffusive filling-in process is restricted to compartments that are formed by BCS boundaries, which create filling-in barriers to by decreasing the permeability of their target gap junctions. The filled-in OFF activities are subtracted from the ON activities at double-opponent cells. In computer simulations of monocular single-scale versions of the BCS/FCS model, double-opponent activities represent the surface brightness of each percept; e.g., Gove *et al.* (1995) and Grossberg *et al.* (1995).
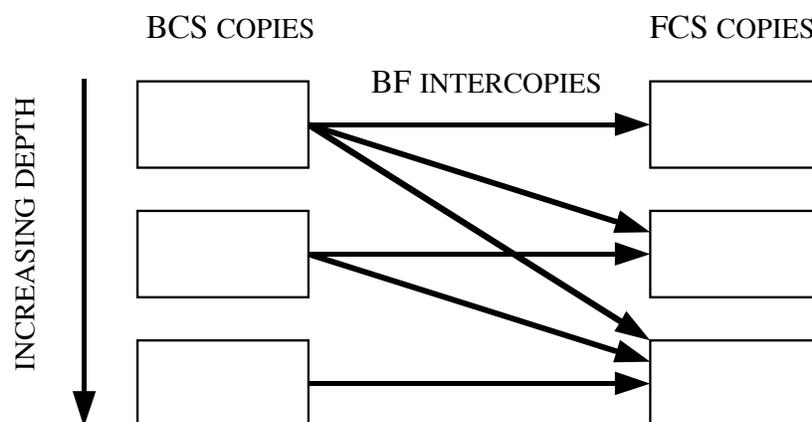
2.3 Binocular Boundary Segmentation by the BCS

The binocular FACADE theory incorporates the monocular BCS mechanisms into a more comprehensive architecture that helps to explain such phenomena as how observers can perceive objects in a scene at different depths; how a partially occluded object can be amodally completed when the occluding object is opaque and modally completed when the occluding object is transparent; and how 2-D pictures can give rise to 3-D percepts of occluding and occluded objects. FACADE theory incorporates the operations of the monocular BCS and FCS into a setting wherein multiple fields of cells, or copies, of the BCS and FCS exist. These copies represent boundaries and surfaces at different relative depths from an observer (Figure 4A). In particular, each BCS copy completes boundaries within its depth range. The multiple FCS copies represent surface representations that can fill-in at the depths of a corresponding BCS copy. Neural principles from which these systems may be derived and their mechanistic realizations were provided in Grossberg (1994). They were mathematically defined and computationally simulated in Grossberg and McLoughlin (1997). Herein a functional description is given of the role that each processing stage plays in generating a final percept. These processing stages are then used to provide a unified explanation of the targeted data.

Figure 5 depicts a macrocircuit of the FACADE theory processing stages. BCS stages are depicted as boxes with vertical lines which designate oriented responses. FCS stages

Figure 4: (A) Each BCS copy generates boundaries within a narrow range of relative depths from the observer. These boundaries act to capture and contain the filling-in of surface brightness and color signals at the corresponding FCS copy. Each FCS copy contains three pairs of opponent Filling-In Domains, or FIDOs. A FIDO is explained in the text. There are both monocular and binocular FIDOs within the model. (B) Within the binocular FIDOs, but not the monocular FIDOs, boundaries corresponding to nearer objects are added to boundaries corresponding to farther objects to prevent farther surfaces from filling-in behind occluding objects. In more technical terms, each FCS copy receives inhibitory boundary-gating signals from one or more boundary contour system (BCS) copies. These signals, called BF intercopies, are partially ordered from nearer to farther BCS copies.

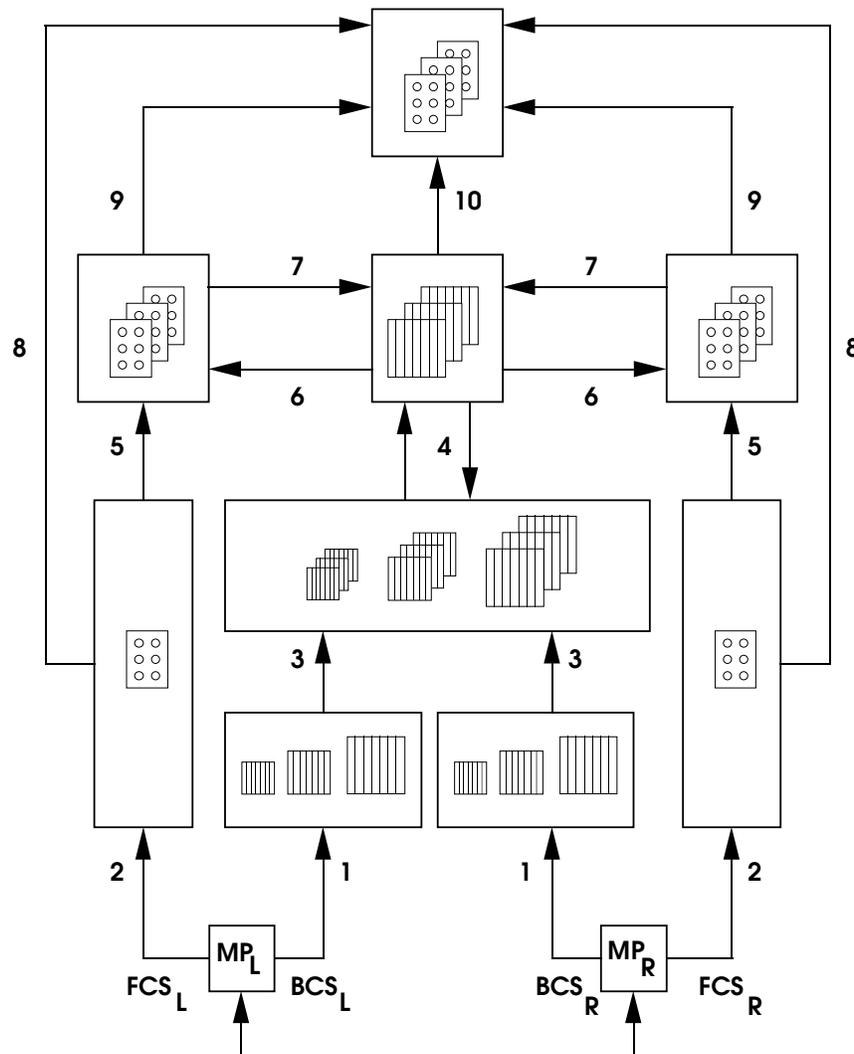Figure 5: Macrocircuit of monocular and binocular interactions of the boundary contour system (BCS) and the feature contour system (FCS). Left eye and right eye monocular preprocessing stages (MP$_L$ and MP$_R$) send parallel pathways to the BCS (boxes with vertical lines, designating oriented responses) and the FCS (boxes with three pairs of circles, designating opponent colors). See text for details.

are depicted as boxes with three pairs of circles which designate opponent colors. Monocular preprocessing of left eye (MP_L) and right eye (MP_R) signals discounts the illuminant before generating parallel inputs to the BCS and FCS via pathways 1 and 2, respectively. Pathways 1 are used to activate BCS simple cells with multiple receptive field sizes. Pathways 2 activate FCS cells that are organized into opponent colors: (red, green), (blue, yellow), (black, white). Pathways 3 carry rectified simple cell inputs to complex cells, as in Figure 3.

BCS interactions are more complicated in the binocular BCS than in its monocular predecessor. For example, simple-to-complex cell interactions define a binocular filter that converts the responses of simple cells with multiple receptive field sizes, or spatial scales, into responses by populations of complex cells to different ranges of binocular disparity in the viewed scene. The complex cells that are activated by larger simple cell scales are capable of fusing a broader range of binocular disparities than are the complex cells which are activated by smaller cell scales. This property is often called the size-disparity correlation (Julesz and Schumer, 1981; Kulikowski, 1978; Richards and Kaye, 1974; Schor and Tyler, 1981; Schor and Wood, 1983; Schor *et al.*, 1984; Tyler, 1975; 1983). As a result of the size-disparity correlation, a single complex cell can respond to a range of binocular disparities, not just a single disparity. Competition across disparity at each position and scale converts this range of possible responses into more sharply tuned actual responses at complex cells.

Output signals from complex cells activate hypercomplex cells, as in Figure 3, via spatial and orientational competition, all within a given scale. These interactions also occur at the processing stage between pathways 3 and 4 in Figure 5. The outcome of these interactions is a set of disparity-tuned, endstopped, and orientationally selected hypercomplex cell responses across multiple spatial scales and positions.

The next operations combine cell computations across multiple *scales* into cell responses that are tuned to different *depths*. By this transformation, multiple-scale responses that obey a size-disparity correlation are combined into responses that selectively code different relative depths of objects from the observer. This scale-into-depth transformation is accomplished by pathways 4 in Figure 5. Here, the outputs from hypercomplex cells across all scales that are tuned to the same depth range converge on shared bipole cells which in turn feed back to the same set of hypercomplex cells. This happens for all the depth ranges, thereby defining multiple CC Loops that are sensitive to different, but possibly overlapping, depth ranges.

2.4   3-D Surface Formation within the FCS

As in the monocular FCS model, illuminant-discounted FCS signals generate a surface representation by initiating filling-in within compartments that are defined by BCS signals. In the monocular model, BCS signals function only as barriers, or obstructions, to the diffusion process which carries out the filling-in. In the full FACADE model, BCS signals to the FCS also carry out a selective function. They are filling-in *generators* as well as filling-in *barriers*. By this means, monocular FCS signals that start out with no depth-selectivity are captured by surface representations that code a prescribed range of relative depths from the observer. The same filling-in process that recovers surface brightness and

color hereby generates a representation of surface depth and form that is imbued with these perceptual qualities.

This surface capture process is modeled as follows. As noted above, there are multiple BCS copies, each corresponding to a range of relative depths from the observer. Each BCS copy generates topographical output signals to a corresponding FCS copy, or small subset of copies, via pathways 6 in Figure 6A. Each FCS copy contains three pairs of monocular Filling-In DOmains, or FIDOs, that correspond to the three pairs of opponent colors. Each FIDO responds to FCS inputs by diffusing them within its BCS boundaries (Figure 6A). The discounted monocular FCS signals are topographically input to *all* the FCS copies by pathways 5 in Figure 5. This one-to-many input process sets the stage for surface capture.

Monocular FCS inputs are captured by a particular monocular FIDO if they are spatially coincident and orientationally aligned with the BCS inputs to that FIDO. Double-opponent cells can carry out the capture property. These double-opponent cells receive their inputs from a pair of FIDOs that represent opponent colors in the manner described below. Captured FCS inputs trigger filling-in of depthful surface representations at the corresponding FIDO. Only surfaces that are surrounded by a connected BCS boundary, or fine web of boundaries, can contain the filling-in process. FCS inputs diffuse out of gaps in boundaries until they are contained by a larger connected boundary or dissipate due to their spatial spread.
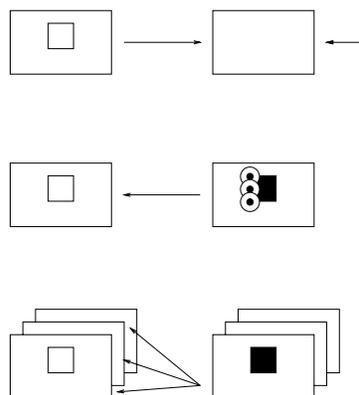

Figure 6: FCS → BCS feedback interactions: (A) BCS boundaries are used to regulate filling-in of surface color in the FCS. (B) A spatial contrast mechanism determines the boundaries of the connected filling-in FCS components. (C) The contrast-based FCS outputs excite BCS cells at the same disparity and position and inhibit BCS cells at smaller disparities at the same position ("boundary pruning").

The total circuit wherein BCS signals input to opponent FIDOs, and the outputs of the FIDOs are filtered by double opponent cells, is called a FACADE filter, because it selects the combinations of Form-And-Color-And-DEpth signals that will fill-in the final surface representation. This surface representation is formed at the binocular FIDOs (top box in Figure 6), where the output signals from the monocular FIDOs are binocularly

matched before triggering surface filling-in. In summary, the FACADE filters generate outputs from their monocular FIDOs only if their monocular FCS inputs are compatible with their binocular BCS boundaries. All other FCS inputs are suppressed.

A brief summary of how FACADE filters selectively capture their surface properties will now be given. Each FIDO consists of a pair of opponent filling-in networks, called syncytia, that activate a double-opponent output network (see Figure 7). Such a double-opponent network consists of four parts: (a) an on-center off-surround network that obeys membrane, or shunting, equations is topographically fed inputs by one syncytium, (b) another on-center off-surround network is topographically fed inputs by the opponent syncytium, (c) boundary signals gate the diffusive flow of filling-in signals across both syncytia, and (d) subtractive opponent interactions occur at each position. between the outputs of the two opponent networks. The output networks are double-opponent networks because the spatial opponency of the on-center off-surround networks is followed by the color-opponency of the cross-syncytial competition.

The on-center off-surround networks generate outputs only at positions where a spatial discontinuity, or sufficiently large gradient, occurs in the level of filled-in activity. This can happen only at positions for which a boundary signal acts as a barrier to the filling-in of activity. Thus, if a depth-selective boundary does not capture a brightness or color signal within its monocular FIDO, then that brightness or color signal cannot generate an output from this monocular FIDO to the corresponding binocular FIDO. This is the first property that helps to selectively capture surface properties at some depths, but not others. Capture can occur only at those depths for which boundaries exist that are spatially coincident with monocular brightness or color signals.

Why are double-opponent interactions needed? They prevent incorrectly matched two-dimensional boundaries and brightness or color signals from generating visible percepts in situations where the single opponent processing of the on-center off-surround networks is not sufficient, notably during binocular rivalry. (See Grossberg, 1994, Sections 45-48 for further discussion of this point). A striking conclusion of this analysis is that the double-opponent cells in the monocular FIDOs function as part of a form-and-color-and-depth filter, and carry no visible brightness or color signal. Rather, they are predicted to generate amodal surface percepts that are used to recognize the surface properties of occluded parts of surfaces, unaccompanied by a conscious visible percept. (See Grossberg, 1997, Section 23, for a further discussion of this point.)

2.5   The Asymmetry Between Near and Far

Before the outputs from the monocular FIDOs can generate a final percept, feedback interactions occur from FCS to BCS, and between BCS and FCS copies that represent different depths. Such interactions realize "the asymmetry between near and far" that is evident in many perceptual data, including data concerning how occluding surfaces gain ownership of boundaries that they share with occluded surfaces, and how occluded surfaces are amodally completed behind modally completed occluding surfaces; see Grossberg (1994, 1997) for examples. This is achieved in the model as follows.

Within a monocular FIDO, only activated regions that are surrounded by a connected boundary or web of boundaries can contain their diffusing activities. Because the output
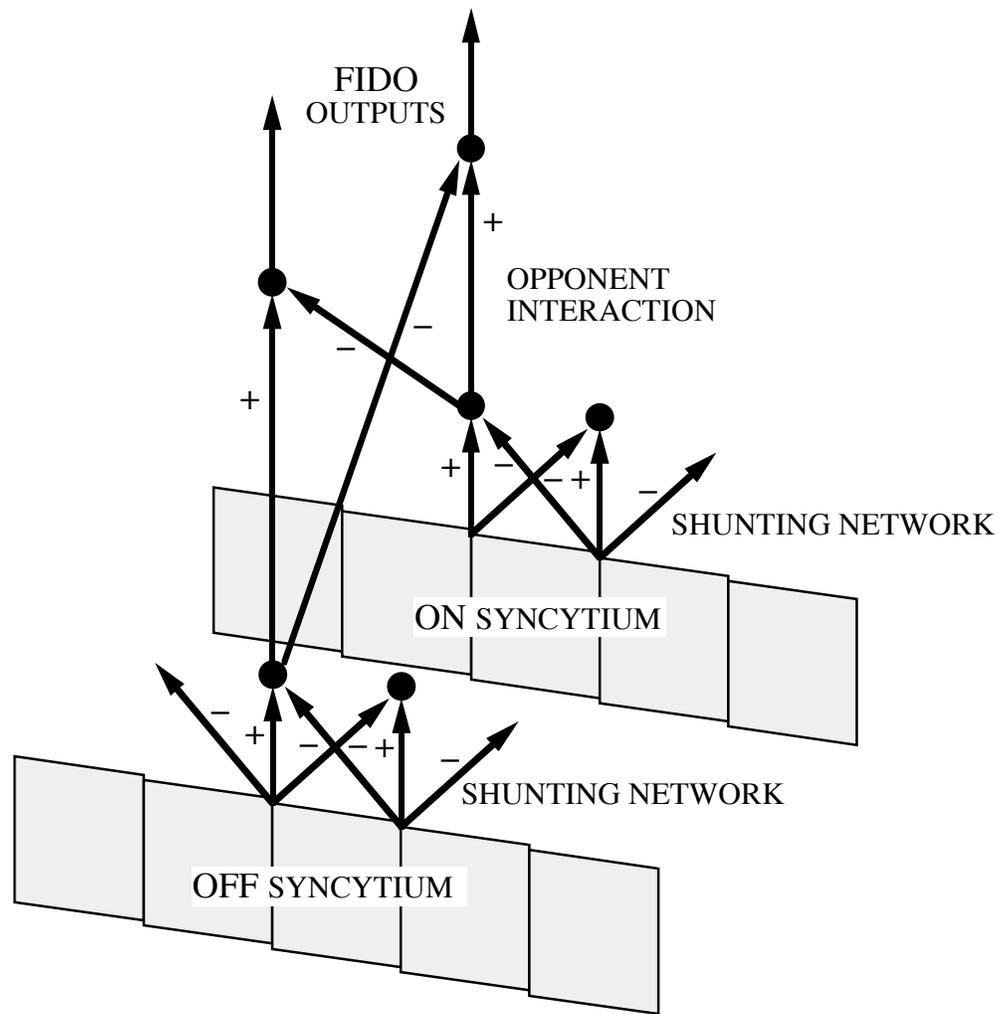
Figure 7: A Filling-In-DOmain, or FIDO: The filled-in activity patterns of the on-syncytium and the off-syncytium are filtered by contrast-sensitive on-center off-surround shunting networks. In addition, the output signals from the shunting nets compete at each position to compute the ON and OFF outputs from their respective FIDOs.

signals of the FACADE filter are contrast-sensitive, they generate output signals at FIDO positions that correspond to connected BCS boundaries. These outputs are carried along two different pathways.

First, they generate FCS → BCS feedback signals along pathways 7 in Figure 5; also see Figure 6B. These signals enhance the BCS boundaries that define the successfully filled-in FCS regions; these boundaries represent the same depths as the corresponding FCS region. The other FCS → BCS feedback signals inhibit boundaries at their positions which correspond to more distant surfaces (Figure 6C). This near-to-far inhibition prunes extra boundaries that were formed due to the size-disparity correlation. When the extra boundaries of occluders are pruned, the boundaries of occluded objects can be completed behind those of occluding objects. The reorganized boundaries then restructure the filling-in within the corresponding FCS surfaces via BCS-to-FCS feedback. This BCS ↔ FCS feedback process realizes a property of boundary-surface consistency.
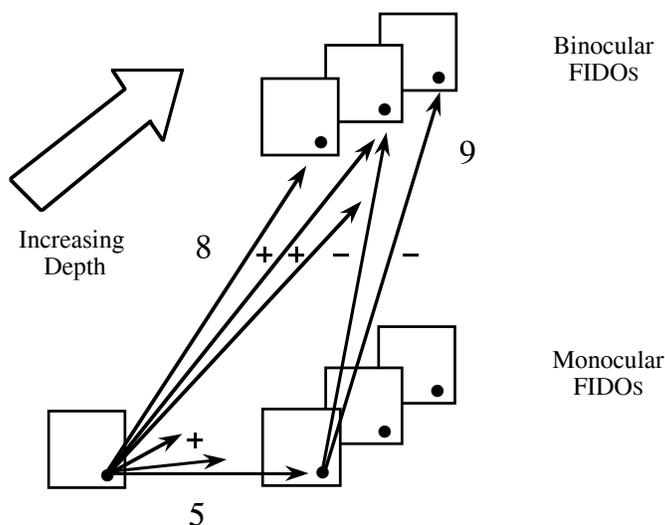

Figure 8: Successfully filled-in surfaces at the monocular FIDOs use pathways 9 to inhibit those binocular FIDOs whose surfaces represent greater distances than their own. This inhibition prevents the same brightnesses and colors from filling-in redundantly at multiple depths.

Second, they generate FCS → FCS signals along pathways 9 in Figures 5 and 8. These signals interact with those along pathways 8, which carry out a one-to-many mapping of FCS signals for binocular matching and surface capture at the binocular FIDOs. Pathways 9 carry out a surface pruning operation that eliminates redundant FCS signals from pathways 8. They hereby prevent occluding objects from filling-in their color at multiple depths.

The boundaries that control depthful filling at the binocular FIDOs also prevent FCS signals outside an occluded region from diffusing behind its occluder. This is accomplished by a boundary enrichment process that adds near boundaries to far boundaries within the binocular FIDOs, as in Figure 4B, along pathways 10 in Figure 5. Thus, within the binocular FIDOs (Figure 4B), but not the monocular FIDOs (Figure 4A), the boundaries of

an occluding object create a barrier to diffusion within the binocular FIDO of its occluded object. Further details of the 3-D model that are relevant to the data at hand are discussed below.

3 Chromatic Texture Segregation: Qualitative Account

Perceived segregation in element-arrangement patterns covaries with the difference in activities within the BCS between the top and bottom regions of the display. For example, if the top region produces only strong vertical signals while the bottom region produces only strong diagonal signals, perceived segregation will be strong. If BCS responses for the top and bottom regions are similar, perceived segregation will be weak. The discussion below assumes that patterns are composed of equiluminant red and blue squares and that backgrounds and interspaces are achromatic.

Figure 9: Explanation of strong segregation on a black background. Top: input pattern. Red (blue) squares are indicated with left (right) diagonal hatched lines. Boundary 1 shows the vertically oriented boundary signals before the effects of FCS to BCS feedback. Boundary 2 shows boundary signals after FCS to BCS feedback. Line thickness designates boundary strength. In both cases, vertical responses are stronger in the top region (indicated by the width of the vertical lines).

The hypothesis that BCS boundary differences help to explain element-arrangement

segregation does not imply that FCS surface properties are unimportant. Indeed, feedback from FCS surface formation processes to the BCS boundaries plays a key role in explaining the BCS patterns. On the other hand, FCS brightness differences have not been needed to capture the main data trends, in keeping with the fact that the red and blue squares are equiluminant.

Figure 9 illustrates how the model explains the strong segregation with a black background. The stages of filtering and grouping (Boundary 1) leading to the initial BCS responses produce strong vertical responses on top due to the vertical arrangement of the red and blue squares. In particular, oriented simple cells are selective for color, so red-sensitive vertical simple cells are more highly activated in the top region of the display, much as in Figure 1B, due to the higher density of contiguous red squares there. A similar fact accounts for the higher activation of vertical blue-sensitive cells in the top region. Strong oblique responses occur on the bottom region due to diagonal arrangement of the red and blue squares there. These initial boundary signals are used to regulate filling-in within the Filling-In DOmains (FIDOs) of the FCS, as in Figure 4. FCS activities provide the basis for surface feedback signals which can potentially contribute to perceived segregation. Surface regions within the FCS that are surrounded by connected boundaries succeed in trapping their filled-in activities. These regions thereby create filled-in activities whose contrast with their surrounds drops off sharply at BCS boundary locations. Within the red FIDOs, these filled-in regions are the red squares, which are surrounded by inactive red cells at all blue square and black background locations. Likewise, within the blue FIDOs, only the blue squares regions fill-in. The black FIDO fills-in the black background with an activity level that is determined by the OFF-contrast. This contrast is small compared to that of the white background. Its effect is therefore omitted in the present simulations for simplicity.

Once the filled-in FCS surfaces emerge, they can generate feedback signals through FCS to BCS pathways (pathways 7 in Figure 5). Because these feedback signals are contrast-sensitive, they occur at the locations of those BCS boundaries at which filled-in activity levels rapidly change across space (see Figure 6). For example, they occur at the edges of the filled-in red squares within the red FIDO. Because the output cells span the spaces between successive squares, they deliver larger positive feedback signals at the top half of the figure, where red squares are contiguous, than at the bottom, where they are not (Figure 9, Boundary 2). In this way, the FCS-to-BCS feedback signals sense the contiguous colinear arrangement of red squares at the top half of the figure, and reinforce BCS boundaries there accordingly. A similar color-selective feedback occurs from blue squares in the blue FIDOs to the BCS. In summary, both the color-sensitive simple cells in the striate cortex and the color-sensitive surface-to-boundary feedback cells in the extrastriate cortex are predicted to strengthen the vertical BCS groupings at the top half of the display, and to thereby support strong segregation.

Achromatic feedback from the filled-in black background to the BCS cannot overwhelm chromatic feedback because its strength is the same at both the top and bottom of the display and covaries with the red and blue luminance levels. This is in contrast to the case of the white background, whose feedback signals far exceed those caused by the red and blue squares, as we now discuss.

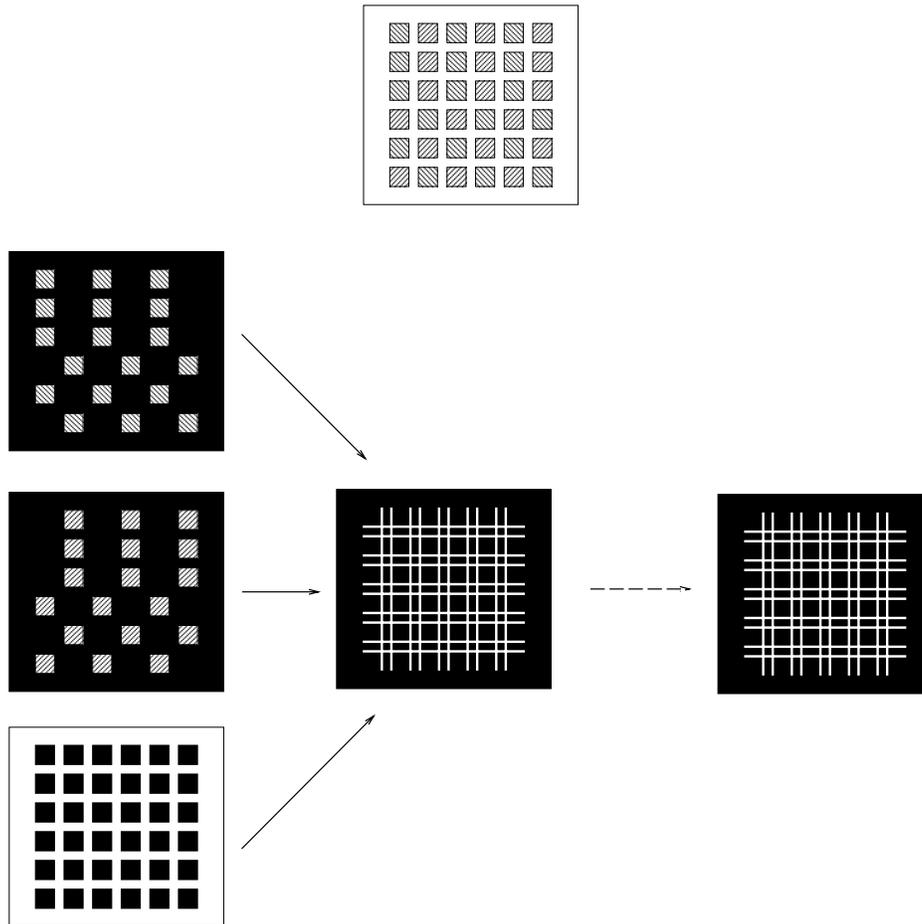Figure 10 illustrates how the model explains the weak segregation with a white back-

Figure 10: Explanation of weak segregation on a white background. Top: input pattern. The high luminance achromatic background creates equally strong boundaries both before (Boundary 1) and after (Boundary 2) FCS-to-BCS feedback.

ground. The high luminance background strongly activates achromatic vertical and horizontal simple cells at both the top and bottom halves of the display. Because the white background is of far greater luminance than the red and blue squares, the advantage of vertical red and blue simple cells at the top half of the figure is overwhelmed by the achromatic simple cell inputs when they are pooled at the complex cells (Figure 3). The white background hereby generates strong horizontal and vertical BCS boundaries that dominate on both the top and bottom regions (Figure 10, Boundary 1). The FCS feedback from the achromatic FIDO to the BCS is also strong because the high luminance of the white background creates a highly contrastive surface representation in this FIDO (Figure 10, Boundary 2). This feedback confirms the vertical and horizontal lattice of BCS boundaries and thereby works against good segregation. FCS feedback from the chromatic red and blue FIDOs to the BCS does favor the vertical groupings on the top region. The red and blue squares, however, are much less luminous than the white background. Thus their feedback signals are weak relative to the achromatic FCS-to-BCS feedback signals, and to the BCS segmentation that is directly generated by the display. Hence, all in all, FCS-to-BCS feedback confirms the initial boundaries and the final boundary signals are similar on top and bottom. Perceived segregation is weak.

Beck (1994) showed that horizontal interspaces interfere more with segregation than vertical interspaces. This result is explained by the model as illustrated in Figures 11 and 12. In both cases, oriented filtering is dominated by the interspaces in both the top and bottom regions due to the high interspace luminance. This effect is mediated by achromatic (Black-White) simple cells. On the other hand, the chromatic (Red-Green, Blue-Yellow) vertical simple cells respond better at the top than the bottom. Here we assume, for simplicity, that these simple cells are blind to achromatic cues. The chromatic and achromatic filter outputs add at complex cells, where responses are dominated by the achromatic inputs, before grouping begins.

Better segregation occurs in the vertical interspace case in part because the chromatic and achromatic vertical groupings on the top summate, whereas they are perpendicular in the horizontal interspace case. In the vertical interspace case, the chromatic vertical groupings on top, albeit weak relative to the achromatic vertical groupings on top and bottom, provide an advantage to the top region after grouping occurs. In the horizontal interspace case the strong achromatic horizontal grouping competes with the weak chromatic vertical grouping in two ways. First, there is competition between perpendicular orientations at the hypercomplex cells (Figure 3). The strong horizontal responses at hypercomplex cells can weaken the vertical responses at the their positions even before the bipole cells are activated. Second, the horizontal interspaces cause horizontal hypercomplex cells to directly inhibit the vertical bipole cell receptive fields (Figure 3). This spatial impenetrability constraint prevents colinear groupings from forming across intervening forms that are not colinear with them. Thus the modest advantage of vertical chromatic simple cells at the top region is weakened by the strong horizontal grouping in the horizontal interspace case.

A similar analysis helps to explain why the vertical interspace bars do not overwhelm the squares as much in Figure 11 as they do when they are part of a white background with both horizontal and vertical interspaces, as in Figure 10. A white background generates strong achromatic horizontal signals that compete with vertical chromatic signals at the

Figure 11: Explanation of segregation for vertical interspaces. Top: input pattern. Boundary 1 signals represent activation before the effects of surface feedback take place. These signals do not support strong segregation and support similar segregations for vertical and horizontal interspaces. Boundary-vertical signals show activities after feedback takes place. These signals support good segregation.
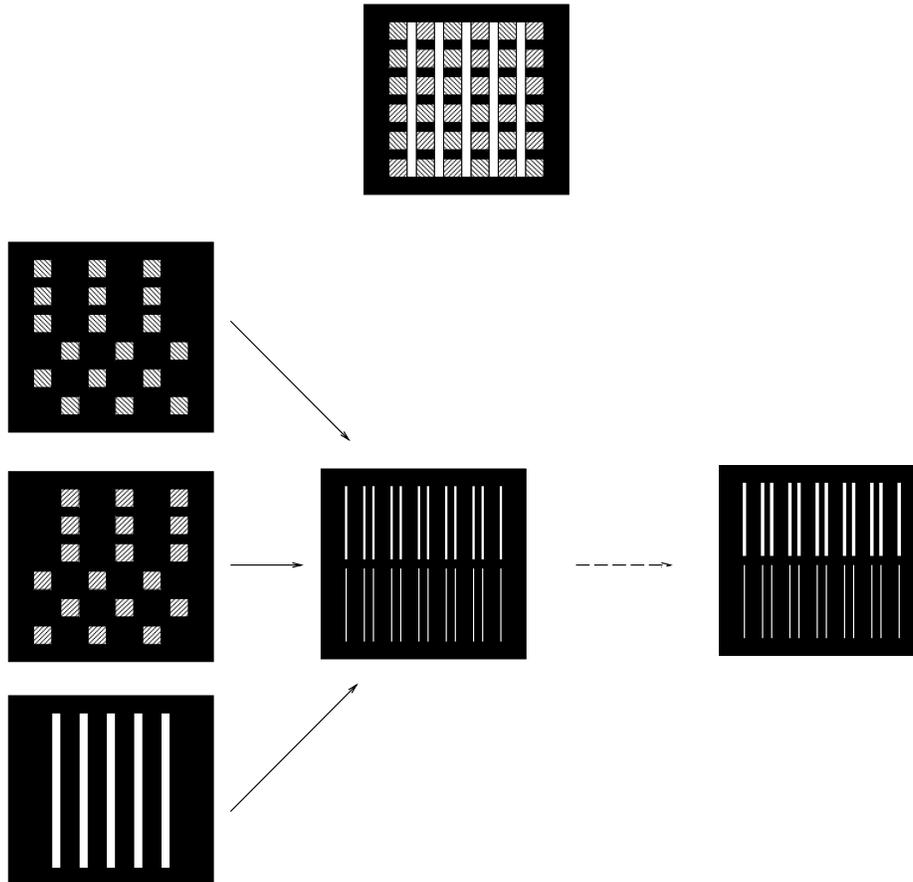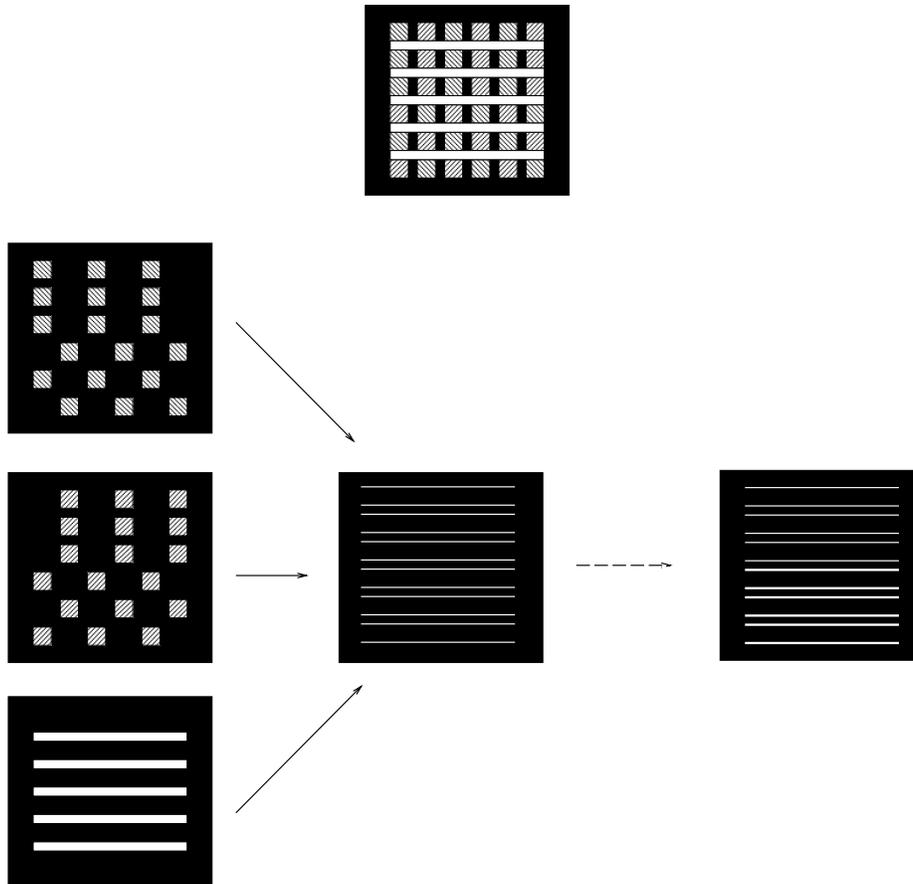
Figure 12: Explanation of segregation for horizontal interspaces. Top: input pattern. Boundary 1 signals represent activation before the effects of surface feedback take place. These signals do not support strong segregation and support similar segregations for vertical and horizontal interspaces. Boundary-vertical signals show activities after feedback takes place. Weak segregation ensues.

hypercomplex cells and at the bipole cells. Given only vertical interspaces, this strong horizontal competition with vertical grouping does not occur.

Surface feedback signals modify these BCS groupings as follows. In the horizontal and vertical interspace cases, there are either strong horizontal or vertical achromatically mediated FCS-to-BCS feedback signals from the filled-in surface representations of the FIDOs. There are also stronger chromatic vertical signals from the Red-Green and Blue-Yellow FIDOs at the top region than at the bottom. In the vertical interspace case, these vertical feedback signals are compatible with other CC loop inputs, including the achromatic vertical FCS-to-BCS feedback signals, so they can generate an advantage for the top region. In the horizontal interspace case, they are nullified by competitive CC loop interactions, including the strong achromatical horizontal FCS-to-BCS feedback signals, at the orientationally-competing hypercomplex cells. In summary, displays containing vertical interspaces segregate better than displays with horizontal interspaces.

Although high luminance horizontal white lines generally produce weak segregation (Beck, 1994), if the lines are seen in front of the red and blue squares through binocular disparity, then segregation is strong (Pessoa and Beck, unpublished results). FACADE theory explains this result through the near to far boundary pruning inhibition that originates in the FCS (Figure 13). Suppose that the disparity manipulation excites cells that are selective for disparities D_1 and D_2, where $D_1 > D_2$. We consider, for definiteness, crossed disparities such that nearer positions generate larger disparities. In particular, suppose that the larger disparity D_1 can fuse the vertical ends of the horizontal white bars. Near-zero disparity cells respond to the horizontal contours of these white bars and are added to those of the vertical disparity D_1 cells. After grouping, a connected boundary forms at the D_1 cells around the horizontal white bars. These D_1 responses are similar in the top and bottom regions, which are both dominated by the strong horizontal signals. The smaller disparity D_2 cells fuse the vertical boundaries of the squares. Near-zero disparity signals add to these D_2 responses and hereby create connected boundaries around the square regions and their black surrounds.

The boundaries produced in this way by initial filtering and grouping are used to regulate depth-selective filling-in. At disparity D_1, only the boundaries that surround the white horizontal lines are connected. Hence, filling-in occurs within the achromatic FIDO. At disparity D_2, the red, blue, and achromatic (black) FIDOs are all surrounded by connected components, and hence fill-in. The black background components are herein ignored because of their negligible effect on grouping. They do, however, contribute to the percept of a smooth surface that joins red and blue squares to their black background at disparity D_2.

FCS-to-BCS feedback is excitatory for cells that correspond to the same depth and inhibitory for cells corresponding to smaller disparities; see Figure 6. Both horizontal and vertical boundaries around the white horizontal bars are hereby strengthened at disparity D_1. The horizontal boundary pruning signals from disparity D_1 to D_2, however, inhibit the D_2 horizontal boundaries. As a result, the horizontal boundaries no longer obstruct colinear grouping of the vertical sides of contiguous squares. These vertical boundaries can cooperate to form longer-range boundaries between the squares that are amodally completed behind the horizontal lines.

In addition, the excitatory chromatic surface-to-boundary feedback within disparity
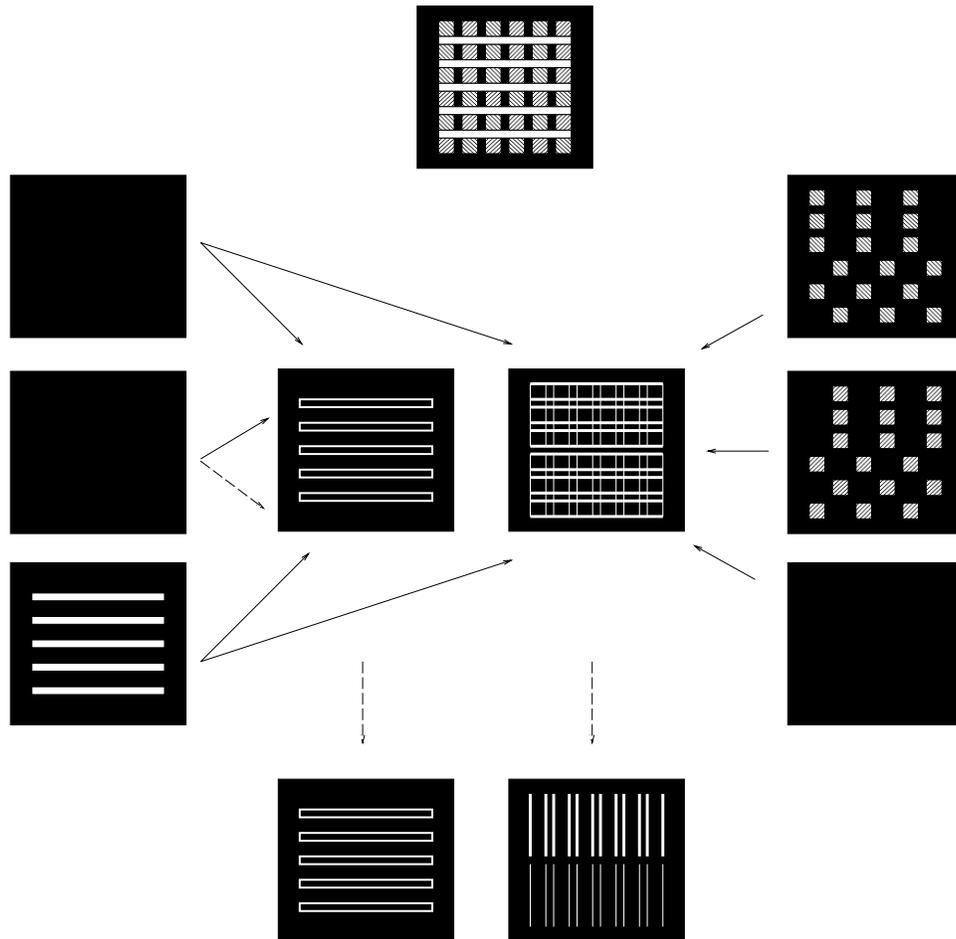
Figure 13: Explanation of strong segregation when horizontal white lines are seen in front. Top: input pattern. Boundary signals in the middle represent activation before the effects of surface feedback take place. Boundary signals in the bottom show activities after feedback takes place. The final boundary activations for disparity D_2 provide the basis for strong segregation.

D_2 favors the vertical grouping on the top half of the display. Competition from the strong horizontal boundaries does not occur, because these boundaries are inhibited within disparity D_2 boundary pruning signals from disparity D_1. Thus strong long-range vertical boundaries form selectively at the top half of the display, abetted by vertical surface-to-boundary feedback.

This explanation of disparity-selective pop-out of the horizontal occluders in front and vertical amodal completion behind the occluders within the top half of the display uses the same mechanisms that Grossberg (1994) used to explain a variety of 3-D pop-out effects in untextured scenes, including Da Vinci stereopsis (Gillam and Borsting, 1988; Kaye, 1978; Lawson and Gulick, 1967; Nakayama and Shimojo, 1990; Wheatstone, 1838) and 3-D neon color spreading (Nakayama, Shimojo, and Ramachandran, 1990). The same mechanisms were also used there to explain pop-out in response to a variety of 2-D pictures, without a disparity manipulation, as in the Weisstein effect (Gillam and Borsting, 1988; Kaye, 1978; Lawson and Gulick, 1967; Nakayama and Shimojo, 1990; Wheatstone, 1838) and the Bregman-Kanizsa effect (Bregman, 1981; Kanizsa, 1979). In these latter explanations, the size-disparity correlation was used to explain how an occluder could selectively activate larger disparity BCS cells which, by near-to-far inhibition, could free slightly smaller disparity cells to carry out amodal completion behind the occluder.

Why does this mechanism not produce better segregation when there are horizontal interspaces in a 2-D picture, as in Figure 12? The answer is that it sometimes does. Such improved segregation can occur due to pop-out of the horizontal interspaces and vertical amodal completion of the red and blue squares in the 2-D case also. It is facilitated, for example, by varying the width of the horizontal bars relative to the height of the squares (see Figure 2B, bottom row). If the squares are larger than the interspaces, then pop-out is facilitated. This can be explained by the fact that the vertical bipoles which group successive squares together can more easily do so when they have a larger support ratio; namely, larger inducers relative to the region to be spanned (Shipley and Kellman, 1992). See Grossberg *et al.* (1997) and Lesher and Mingolla (1993) for a discussion of how bipole cells can generate stronger illusory contours as the support ratio increases. Attention to the interspaces may also facilitate pop-out. Within the theory, such an attention shift differentially strengthens the horizontal interspace boundaries relative to the competing vertical boundaries and aids the pop-out process using the same mechanisms as in Grossberg (1994). The horizontal interspace case may thus give rise to better or poorer segregation than the vertical interspace case, depending upon whether the displays favors pop-out or not. The main point about a disparity manipulation is that it can cause good segregation even in cases where segregation to the 2-D image is poor.

As noted above, segregation of element-arrangement patterns on a white background is weak (Beck, 1994). Pessoa *et al.* (1996) have shown that when a disparity manipulation causes the squares to be seen in front of a white background, then segregation does not greatly improve. This result is challenging because disparity-based pop-out does greatly improve segregation in the case of white horizontal interspaces. FACADE theory explains this finding in the manner summarized by Figure 14. Again, two pools of disparity selective cells are invoked, D_1 and D_2, as well as near-zero disparity cells. The larger disparity D_1 cells can fuse the vertical sides of the squares. Horizontal boundaries of the squares are also present since near-zero disparity signals are added to the vertical boundaries. Together

they form square boundaries at disparity D_1 after grouping occurs. In addition, vertical groupings between vertical square edges can more easily form at the top of the display than the bottom because the red and blue simple cells feed larger intersquare signals to their disparity D_1 complex cells there. The strength of these groupings is modest, however, because of the relatively low luminance of the red and blue squares.
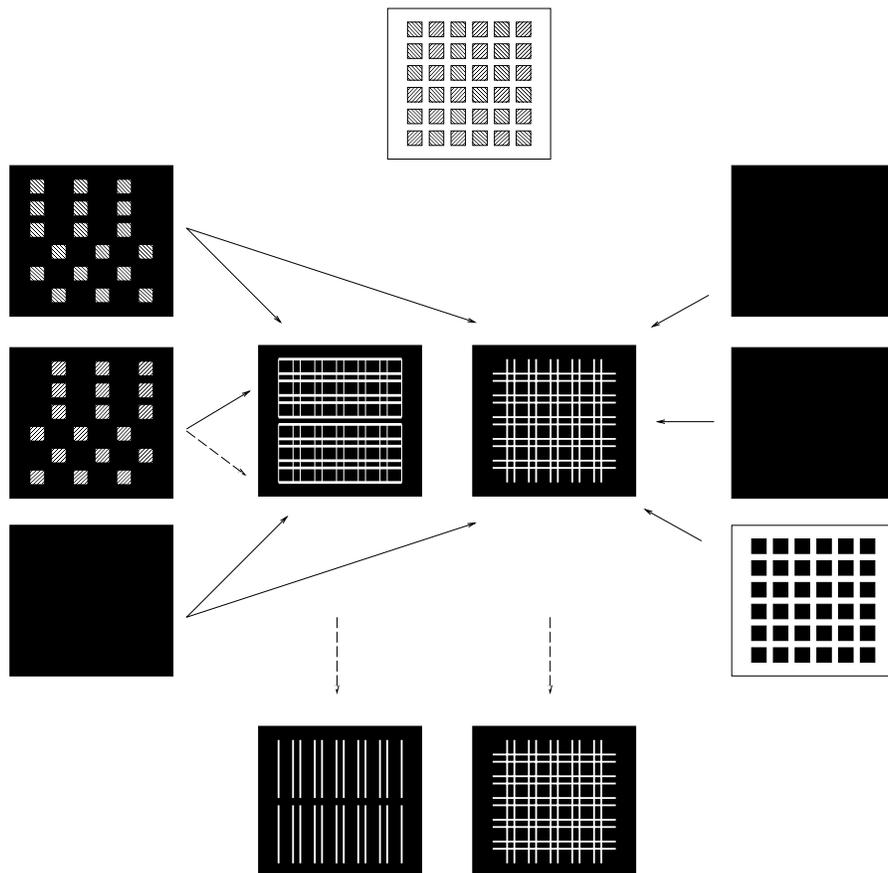

Figure 14: Explanation of weak segregation when the squares are perceived in front of a white background. Top: input pattern. Boundary signals in the middle represent activation before the effects of surface feedback take place. Boundary signals in the bottom show activities after feedback takes place. The final boundary activations for fields D_1 and D_2 do not produce strong segregation.

Disparity D_2 cells are, in contrast, strongly activated by the high luminance vertical contours of the background. Near-zero disparity horizontal boundaries are added to these vertical boundaries to complete the connected boundary frame around the white background after grouping occurs. These are registered at disparity D_2 because the patterns used by Pessoa *et al.* (1995) contained a "micro-textured" background (see Figure 2B). These boundary signals are then used to regulate filling-in.

Surface-to-boundary feedback for the disparity D_1 field more or less preserves the initial boundary activations. In particular, positive feedback from the low-luminance red and blue FIDOs to the corresponding disparity D_1 boundaries modestly strengthens the groupings at the top half of the display.

Negative boundary pruning feedback from the disparity D_1 FIDOs to the disparity D_2 boundaries also occurs. However, this contrast-sensitive feedback is not strong enough to inhibit the strong achromatic horizontal and vertical boundaries of the interspaces, especially since they are enhanced by much stronger excitatory surface-to-boundary feedback within disparity D_2 from the achromatic FIDO that represents the interspace background. In all, although there is a weak vertical advantage at the top of the display in disparity D_1, strong horizontal and vertical groupings occur throughout the display at disparity D_2. The strong vertical groupings at the bottom and top of the display are proposed to interfere with the weaker vertical segregation at the top. Such interference does not occur when viewing near horizontal interspaces, because the far verticals experience no interference from near verticals.

Perceived segregation is, however, strong when the squares are seen in front of a black background (Pessoa *et al.*, 1996). FACADE theory explains this finding as above, with the difference that there is no strong interference from vertical and horizontal boundaries at the disparity D_2. In particular, the vertical disparity D_1 groupings between the top squares can, in this case, inhibit potentially competing background verticals via near-to-far inhibition.

The explanation of why the introduction of depth does not improve segregation when the squares are seen in front, but improves segregation when horizontal lines are seen in front, illustrates a key principle of FACADE theory; namely, that interactions are *partially ordered* from near-to-far depths; e.g., Figures 4B and 6C. These near-to-far interactions have been used to help explain a variety of challenging 3-D percepts that do not involve textured scenes; see Grossberg (1994, 1995) for examples.

FACADE theory has also suggested some new displays whereby to test its mechanisms. Figure 2A (bottom row) shows two stimuli composed of vertical and horizontal white segments. For many display parameters, the display with vertical segments segregates better than the one with horizontal segments. The explanation of FACADE theory of this result is similar to the one given for vertical and horizontal interspaces. First consider patterns with horizontal white segments. On the top half of the display, by spatial impenetrability, horizontal groupings produced by the white segments compete with the vertical groupings produced by the red and blue squares. No orientation is clearly favored. In the vertical segment case, the chromatic and achromatic vertical groupings summate on the top half of the display. Surface feedback further amplifies the vertical advantage at the top half of the display for the vertical segments case. In the horizontal segments case, this advantage is nullified by competitive CC loop interactions. In all, perceived segregation is better for displays with vertical segments than for displays with horizontal segments.

As discussed above, for proper display parameters, patterns with horizontal white interspaces (but no disparity) can lead to improved segregation due to pop-out and amodal completion; for example, if the horizontal interspaces are made narrower. If in such displays, small white vertical segments are added to the horizontal white interspaces, segregation becomes weaker (see Figure 2B, bottom row). This weakening cannot be simply attributed

to the fact that a larger display area is now white (horizontal interspaces plus segments). Informal observations have shown that patterns containing small vertical segments produce weaker segregation than patterns with only horizontal lines when the overall white area is equated in both patterns. Patterns with small vertical segments illustrate a situation where the local geometry can modify pop-out and amodal completion in element-arrangement patterns.

In FACADE theory this is explained as follows. The horizontal boundaries cannot group across the vertical segments, due to spatial impenetrability. This prevents long horizontal boundaries from forming. Instead, the boundaries of the white regions track their horizontal and vertical contours. As in the case of narrow horizontal interspaces, these boundaries can pop-out. When they do, they generate boundary pruning signals to BCS copies that represent larger depths. The vertical boundary pruning signals inhibit the vertical boundaries of the red and blue squares on these BCS copies. This inhibition prevents the red and blue squares from completing vertical boundaries behind the white occluders in the top half of the image. The absence of these vertical groupings reduces the advantage of the top relative to the bottom that narrow horizontal interspaces cause in the absence of vertical segments.

4 Chromatic Texture Segregation: Computer Simulations

The qualitative accounts of chromatic texture segregation presented above were confirmed in a computer implementation of FACADE theory. The simulated mechanisms constitute a subset of the full implementation of Grossberg and McLoughlin (1997). Our implementation was used to capture the main model properties while simplifying its use for other practitioners. This simplification also made the simulations of bipartite textures manageable. In Grossberg and McLoughlin (1997) disparity processing and 3-D grouping were simulated in greater detail, but only achromatic patterns were considered. Here, three fields of Red-Green, Blue-Yellow, and Black-White cells are needed. The disparity and grouping equations were simplified accordingly. Figure 15 shows the model stages employed. The Appendix lists the model equations and parameters.

Stimulus Distribution

Three fields of units arranged as two-dimensional grids sample the luminance distribution and correspond to Red-Green, Blue-Yellow, and Black-White opponent inputs.

Center-Surround Units

The inputs are processed by cells with circular concentric receptive fields that model requisite properties of lateral geniculate cells. In the present implementation, only on-center off-surround, or ON-cells, are employed; see Grossberg and Wyse (1991) and Grossberg *et al.* (1994) for the use of both ON-cells and OFF-cells. The mathematical specification of the receptive fields (see Appendix) uses feedforward equations that undergo membrane equations, or shunting, interactions. A shunting on-center off-surround network computes Weber-law modulated contrast ratios while normalizing the output dynamic range. In effect, it discounts the illuminant and tracks image reflectances.
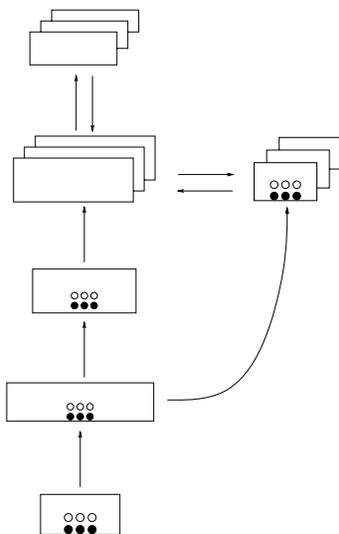
Figure 15: Computational stages of current FACADE implementation. The three pair of circles designate Red-Green, Blue-Yellow, and Black-White opponent colors. Multiple boxes designate multiple fields that correspond to different, but possibly overlapping, depth ranges.

Three fields of ON-cells were employed: Red-Green, Blue-Yellow, and Black-White. Only patterns composed of red and blue squares were simulated. The Red-Green and Blue-Yellow ON-cells can thus be seen as approximations to double-opponent cells at higher processing levels. For example, a R^+G^-/R^-G^+ double-opponent cell becomes R^+/R^- since there are no inputs stimulating the green mechanisms. Consequently, no explicit double-opponent computation is carried out at the subsequent FCS stages.

Simple Cells: Oriented Direction-of-Contrast Sensitive Units

The ON-cells input to model simple cells that are sensitive to luminance contrast of a given orientation and a given contrast polarity, or direction of contrast. For each orientation, there are six cells, corresponding to three opponent fields: L/D (light-dark), D/L (dark-light), R^+/R^- (red-increment/ red-decrement), R^-/R^+ (red-decrement/red-increment), B^+/B^- (blue-increment/blue-decrement), B^-/B^+ (blue-decrement/blue-increment).

Complex Cells: Oriented Polarity Pooling Units

Model complex cells are sensitive to orientation and amount of contrast but pool across contrast and color; that is, they are generalized contour detectors (Thorell, de Valois, and Albrecht, 1984). For a given orientation, complex cells at every position are obtained by summing the half-wave rectified activities of all six types of simple cells within each orientation. In effect, complex cells are sensitive to the sum of the full-wave rectified outputs from the three color channels. Model complex cells are also binocular. In a full implementation of the BCS, complex cells input to hypercomplex cells that compete across position and orientation. These interactions are omitted for simplicity. The orientational competition that realized spatial impenetrability at the bipole cells (Cooperative-Competitive loop) is sufficient to qualitatively explain the targeted data. Thus, in the present simplified model, complex cells receive two sources of top-down input: signals from the CC loop that

originate from BCS grouping, and signals from FCS surface representation. Two fields of disparity selective cells, D_1 and D_2 ($D_1 > D_2$), are used in the BCS: Cells at disparity D_1 are excited by CC loop and surface signals of the same disparity. Cells at disparity D_2 are also excited by CC loop and surface signals of the same disparity. In addition, they are inhibited by D_1 boundary pruning signals from the FCS.

Cooperative-Competitive Loop

The initial, feedforward, complex cell activities that originate from simple cells are used as inputs to the CC loop, which instantiates a spatially long-range cooperative-competitive grouping process. Each bipole cell receptive field is composed of two oriented lobes that receive input from a range of almost colinear orientations and positions that gather evidence for boundary completion at the cell. Both bipole lobes must be sufficiently active for the cell to fire, ensuring that boundaries do not extend beyond line ends unless there is evidence for such a linkage, such as from a second aligned line.

Monocular Filling-in Domains

The monocular FIDOs of the FCS receive two types of input: (1) illuminant-discounted signals of brightness and color that come from the monocular preprocessing stage (center-surround units in the present implementation); (2) depth-specific boundary signals from the BCS (complex cells). Boundary signals are used to regulate the diffusion process that produces filled-in surface regions.

Outputs from the FIDOs are sensitive to spatial contrast. By this means, the contours of the filled-in connected components are fed back to the BCS (see Figure 6). These FCS to BCS signals are excitatory for cells at the same disparity and inhibitory for cells selective for smaller disparities.

Behavioral Linking Hypothesis

The strength of perceived segregation in element-arrangement patterns was assumed to correspond to the *difference* in activities within the BCS (complex cells) between the top and bottom regions of the display. For example, if the top region produces strong vertical signals while the bottom region produces only weak vertical signals, or if the top produces only strong vertical signals while the bottom region produces only strong diagonal signals, then perceived segregation will be strong. If BCS responses for the top and bottom regions are similar, then perceived segregation will be weak. The results are summarized in Table 1. The numerical ratings of segregations in Table 1 have an ordering that qualitatively matches the relative segregation reported by human subjects. The following simulations illustrate how these results were obtained.

Segregation on a black background is strong. This property initiates with the strong vertically oriented responses in response to the top region when compared to the bottom region. In the model, complex cell responses dependent on only feedforward components already support strong segregation (Figure 16). When the background is white, segregation is weak because the achromatically driven BCS groupings on top and bottom are similar. Figure 17 shows the sum of the initial (no CC loop or surface feedback) complex cell responses for the four orientations employed. Activities for the top and bottom regions are similar.

Segregation is stronger for vertical interspaces than for horizontal interspaces. As discussed above, the initial filtering responses and CC loop groupings are insufficient to
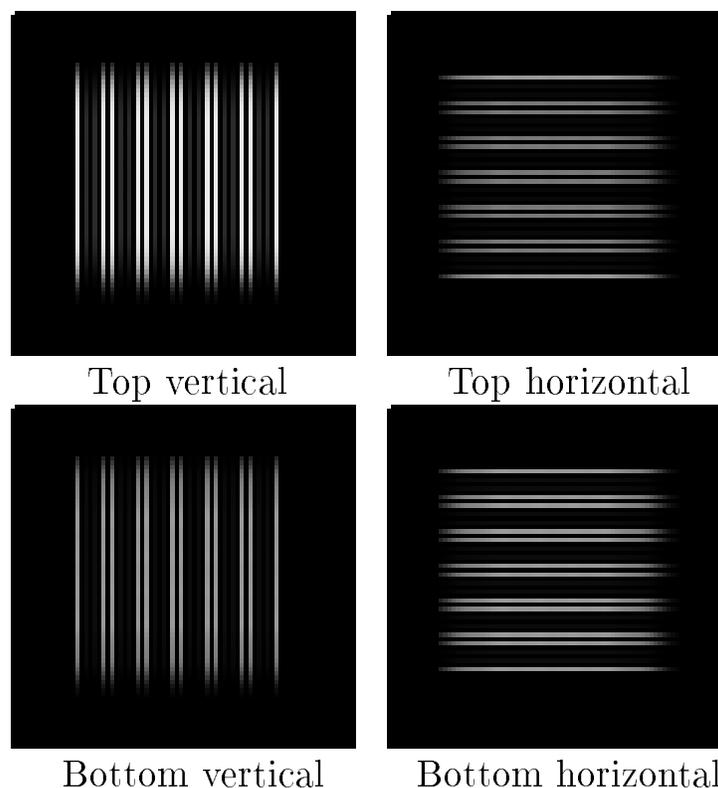
Figure 16: Segregation on a black background is strong. Complex cell activities (feed-forward only) for horizontal cells are similar on top and bottom. Vertical responses are stronger on top and produce strong segregation.

account for the result. Surface feedback mechanisms provide an advantage for vertical groupings on the top region when vertical interspaces are present (Figure 18).

So far we have shown how the model accounts for the basic findings of Beck (1994): Chromatic element-arrangement segregation is strong for a black backround and weak for a white background, and segregation is stronger for vertical interspaces than for horizontal interspaces. Beck (1994) also showed that segregation is inversely proportional to inter-space luminance. As the luminance of the entire background, or the luminance of the vertical or horizontal interspaces, is increased, segregation strength decreases. Moreover, perceived segregation decreases more and in a similar manner when either the luminance of the entire interspace or the luminance of the horizontal interspaces is increased than when the luminance of the vertical interspaces is increased (See Figure 19A) – accordingly, segregation for vertical interspaces is stronger than for horizontal interspaces. Figure 19B shows that the model is able to capture the main trends of the experimental data. In all instances, perceived segregation is inversely proportional to the luminance of the inter-space area, and vertical interspaces produce stronger segregation than entire interspace or horizontal interspace (the latter two produce similar segregation).

When horizontal white lines are seen in front of the squares, segregation is strong (Figure 20). However, when the squares are perceived in front, segregation does not

Stimulus	Segregation (M)
Black background	45.73
White background	20.85
Horizontal lines	25.17
Vertical lines	35.57
Horizontal lines in front	49.94
Squares in front (white background)	19.06
Squares in front (black background)	54.33

Table 1: Segregation strengths. Equation 21 was applied to the final boundary activities for fields D_1 and D_2. The first four cases do not involve depth and therefore segregation is the same for D_1 and D_2. The last three cases involve depth.
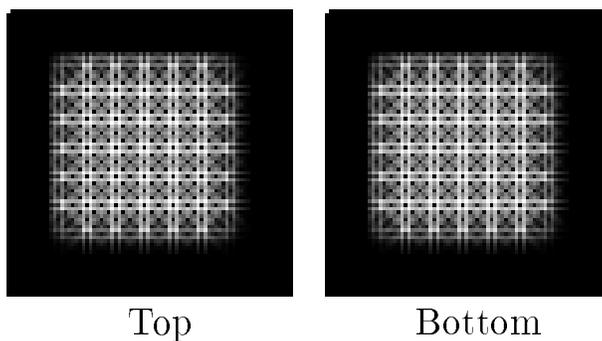

Top   Bottom

Figure 17: Segregation on a white background is weak. Feedforward complex cell responses summed across orientations are similar on top and bottom.

greatly improve. As illustrated in Figure 17, top and bottom groupings are similar when the background is white. The Appendix describes how the segregation ratings in Table 1 were computed from patterns such as those shown in Figures 16–18 and 19.

5 Conclusion

Current visual filtering models propose that rapid texture segregation is determined by the properties of early filtering mechanisms. Evidence from psychophysical and neurophysiological studies indicate that beyond this early filtering stage are stages of boundary segmentation and surface representation (Gibson, 1950; He and Nakayama, 1994; Kanizsa, 1979; Nakayama and Shimojo, 1990; Peterhans and von der Heydt, 1989; von der Heydt et al., 1984). For example, the study of He and Nakayama (1994) showed that manipulations with little effect on early filtering but strong influence on surface representation (e.g., amodal completion) could drastically affect the results of texture segregation. They conclude that the "visual system cannot ignore information regarding surface layout" in

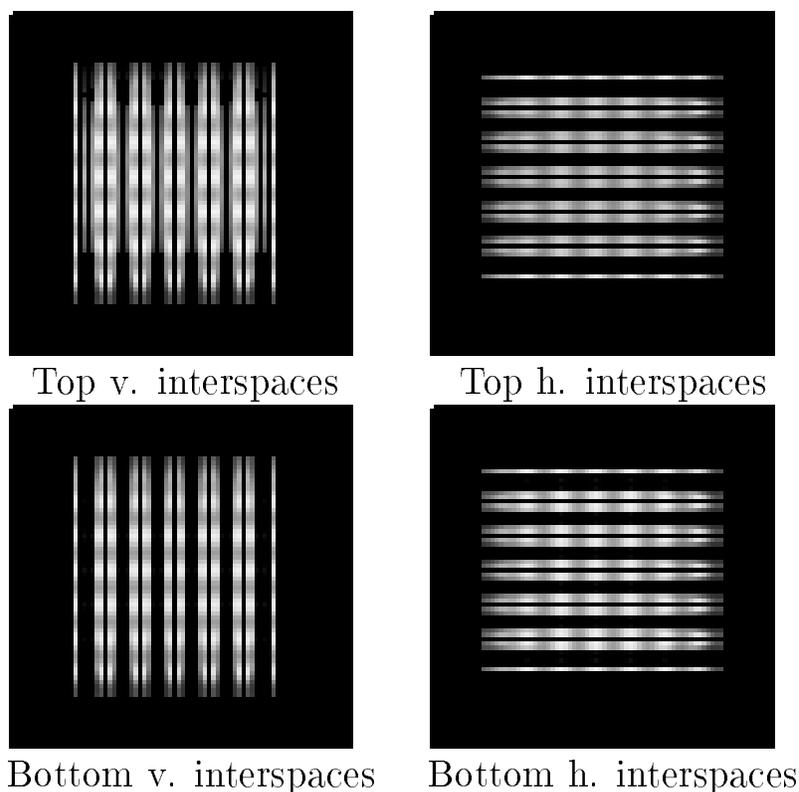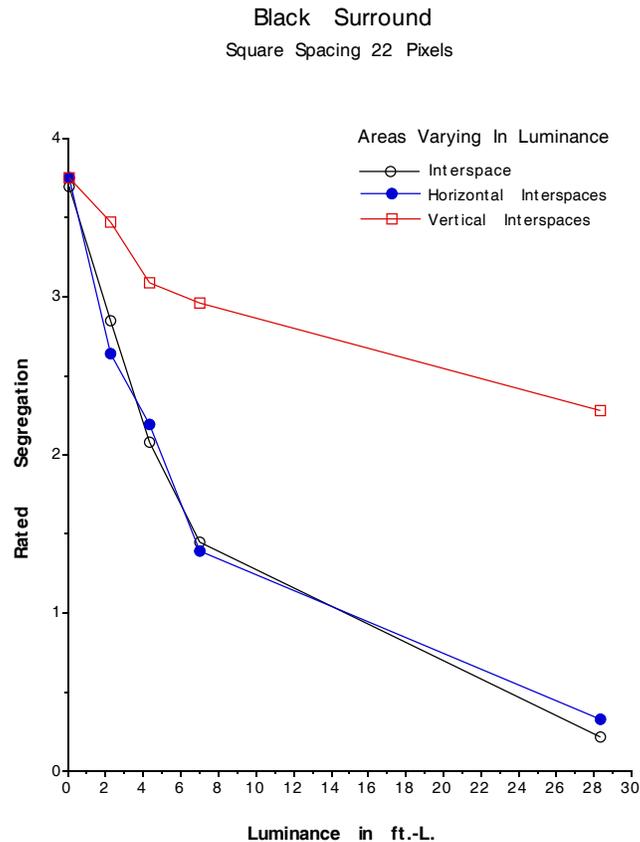| Top v. interspaces | Top h. interspaces |
| Bottom v. interspaces | Bottom h. interspaces |

Figure 18: Segregation with vertical interspaces is stronger than with horizontal interspaces. Final BCS activities after surface feedback. Left: Vertical responses when vertical interspaces are present. Activities are stronger on top. Right: Horizontal responses when horizontal interspaces are present. Activities are similar on top and bottom.

rapid texture discrimination (p. 151).

The results of Beck (1994) and Pessoa *et al.* (1996) on the chromatic segregation of element-arrangement patterns also pose challenges to current theories of texture segregation. The current paper showed how FACADE theory can account for these results by supplementing filtering by both boundary grouping and surface representation mechanisms. In particular, it was shown how the feedback between boundary and surface representations helps to achieve computational consistency between boundaries and surfaces in depth. These interactions are central to our explanations of perceived segregation and have been used by now to account for many other types of data concerning 3-D vision and figure-ground segregation (Grossberg, 1987b, 1994, 1997; Grossberg and McLoughlin, 1997).

(A)

(B)

Figure 19: (A) Mean segregation ratings plotted as a function of luminance in Experiment 1 from Beck (1994). Perceived segregation is inversely proportional to background luminance. The center-to-center spacing of the squares was 22 pixels, and the surround was black. The results shown are for red and blue squares set at 2.3 fL when the luminances of the interspace, the horizontal interspaces between the rows of a texture pattern, and the vertical interspaces between the columns of a texture pattern were varied. [Reprinted with permission from Beck, 1994]. (B) Computer simulation of these data. The same trends observed in the data can be identified.

Top D_1 Top D_2

Bottom D_1 Bottom D_2

Figure 20: Segregation when horizontal interspaces are seen in front is strong. Final BCS activities after surface feedback for fields D_1 and D_2. For t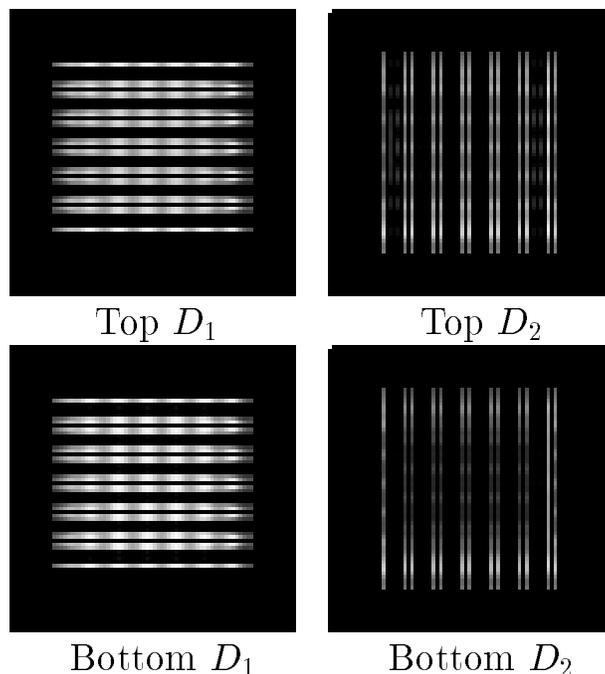he larger disparity D_1, horizontal responses dominate on top and bottom and do not support strong segregation. For the smaller disparity D_2, vertical groupings on top are stronger than on bottom. Perceived segregation is strong.

6   Appendix: Model Equations

Stimulus Distribution

Three fields of units arranged as a two-dimensional grid sample the luminance distribution and correspond to Red-Green, Blue-Yellow, and Black-White opponent inputs: I_{ij}^R, I_{ij}^B, and I_{ij}^A. The superscript denoting the field type will be omitted in the equations below in order to simplify the notation.

Center-Surround Units

The input pattern is processed by ON-cells which obey membrane, or shunting, equations. Filtering is performed in three fields: Red-Green, Blue-Yellow, and Black-White. All fields obey equations of the form (field type omitted)

$$\frac{dx_{ij}}{dt} = -\alpha x_{ij} + (\beta - x_{ij})A_{ij} - (x_{ij} + \gamma)B_{ij}, \qquad (1)$$

where y_{ij} is the activity, or potential, at grid location (i, j); α is the passive decay rate, β the excitatory saturation point, and γ the inhibitory saturation point; A_{ij} is the total

excitatory input to y_{ij} and B_{ij} is the total inhibitory input to y_{ij}. Terms A_{ij} and B_{ij} denote discrete convolutions of the input I_{ij} with spatial weighting functions, or kernels, as in

$$A_{ij} = \sum_{pq} I_{pq} A_{pqij} \quad \text{and} \quad B_{ij} = \sum_{pq} I_{pq} B_{pqij}, \tag{2}$$

where the weighting functions are defined by normalized Gaussians for the center and surround mechanisms, as in

$$A_{pqij} = \frac{1}{\sigma_c \sqrt{2\pi}} \exp\left(-\frac{(p-i)^2 + (q-j)^2}{2\sigma_c^2}\right) \tag{3}$$

and

$$B_{pqij} = \frac{1}{\sigma_s \sqrt{2\pi}} \exp\left(-\frac{(p-i)^2 + (q-j)^2}{2\sigma_s^2}\right). \tag{4}$$

In (3) and (4), $\sigma_s > \sigma_c$ (the surround is broader than the center).

ON-responses are solved at equilibrium (i.e., $dx_{ij}/dt = 0$) and half-wave rectified so that the output X_{ij} satisfies

$$X_{ij} = \left[\frac{\beta A_{ij} - \gamma B_{ij}}{\alpha + A_{ij} + B_{ij}}\right]^+, \tag{5}$$

where $[\omega]^+ = \max(\omega, 0)$. The parameters are $\alpha = 0.1$, $\beta = 4.0$, $\gamma = 4.0$, $\sigma_c = 0.7$ and $\sigma_s = 1.4$.

Simple Cells

Simple cells are obtained, for simplicity, by convolving the ON-responses of a given opponent field with difference-of-offset-Gaussian (DOOG) filters (Grossberg and Todorović, 1988). The elongated Gaussians are given by

$$G_{pqijk} = \frac{1}{2\pi\sigma_h\sigma_v} \exp\left\{-\frac{1}{2}\left(\left(\frac{(p-i)\cos(\frac{\pi k}{12}) - (q-j)\sin(\frac{\pi k}{12})}{\sigma_h}\right)^2 + \left(\frac{(p-i)\sin(\frac{\pi k}{12}) + (q-j)\cos(\frac{\pi k}{12})}{\sigma_v}\right)^2\right)\right\} \tag{6}$$

where σ_v and σ_h define the vertical and horizontal elongations, respectively. Four orientations k were employed: vertical, horizontal, and two 45 degree obliques ($k = 0, 3, 6, 9$). DOOG filters were obtained by using the appropriately shifted oriented Gaussians. For example, for vertically oriented Gaussians, light-dark (LD) and dark-light (LD) kernels are obtained as in

$$G_{pqijk}^{LD} = G_{pqijk} - G_{p+1,qijk}, \tag{7}$$

and

$$G_{pqijk}^{DL} = G_{p+1,qijk} - G_{pqijk}. \tag{8}$$

Thus for each orientation there are six cells, corresponding to three opponent fields:

L/D (light-dark), D/L (dark-light), R^+/R^- (red-increment/red-decrement), R^-/R^+ (red-decrement/red-increment), B^+/B^- (blue-increment/blue-decrement), B^-/B^+ (blue-decrement/blue-increment).

The simple cell output is derived by filtering the ON-responses with a DOOG kernel, thresholding, and nonlinearly compressing the result. Thus, the output is given by

$$s_{ijk}^{F,P} = f([r_{ijk}^{F,P} - T]^+), \tag{9}$$

where F denotes field type (R, B, and A), P is the cell polarity (LD and DL), T is an output threshold, and $r_i^{F,P}$ is given by

$$r_{ijk}^{F,P} = \sum_{pq} X_{ij} G_{pqijk}^P. \tag{10}$$

The signal function f in (9) is a sigmoid of the form

$$f(\omega) = \frac{\omega^n}{A^n + \omega^n}, \tag{11}$$

where A is a constant and $n = 3$. The parameters are $\sigma_h = 0.5$, $\sigma_v = 3.5$, and $A = 0.3$.

Complex Cells

Complex cells pool across directions of contrast and opponent colors. For a given orientation, complex cells activations at every position are obtained by summing the activities of all six simple cells specified above. Complex cell responses are also binocular and receive two extra sources of input: boundary completion signals B_{ijk} from the CC loop and signals F_{ijk} (excitatory) and G_{ijk} (inhibitory) from the surface representations. Two disparities, $D_1 > D_2$, are used. For the larger disparity, D_1, the complex cells obey

$$\frac{dc_{ijk}^{D1}}{dt} = -Ac_{ijk}^{D1} + (B - c_{ijk}^{D1})(S_{ijk}^R + S_{ijk}^B + S_{ijk}^A + \gamma B_{ijk} + \kappa F_{ijk}), \tag{12}$$

where the S_{ijk} signals are the sum of the opposite polarity simple cells for the Red-Green (R), Blue-Yellow (B), and Black-White (A) fields; namely,

$$S_{ijk}^F = s_{ijk}^{F,LD} + s_{ijk}^{F,DL}, \tag{13}$$

where F denotes field type. For all simulations not involving depth, only complex cells obeying equation (12) were implemented.

By (12), complex cells at the largest disparity D_1 do not receive any FCS inhibition but do receive excitatory same-disparity FCS signals (κF_{ijk}). For simplicity, for all simulations not involving depth it was assumed that

$$F_{ijk} = S_{ijk}^R + S_{ijk}^B + S_{ijk}^A. \tag{14}$$

In other words, the FCS output was assumed to be the summed across contrast and color simple cell signals. In a complete implementation of FACADE theory, FCS-to-BCS

feedback would derive from the filled-in regions in FIDOs that are registered by a contrast detection process (see Figure 6B). This process signals the contours of the connected regions of the FIDOs. For the present implementation, given the type of input patterns processed by the system, the contrast-sensitive feedback signal is assumed to be proportional to the contrast-sensitive activities of simple cells. This assumption is plausible because the simple cells and the surface-to-boundary feedback cells are both assumed to compute the oriented contrast of each channel (Red-Green, Blue-Yellow, Black-White), taken separately. Each FIDO computes its own contrast that scales with its color or luminance input, before all these contrast-sensitive outputs summate at target BCS cells.

FCS-to-BCS feedback is depth-selective, and for the two cases involving depth, the F_{ijk} signals for the larger disparity D_1 were given as indicated in Figures 13 and 14. More precisely, for the simulation of white horizontal lines in front

$$F_{ijk} = S_{ijk}^A, \tag{15}$$

and for the simulation where the squares are seen in front

$$F_{ijk} = S_{ijk}^R + S_{ijk}^B. \tag{16}$$

For the smaller disparity, D_2, complex cells obey

$$\frac{dc_{ijk}^{D2}}{dt} = -Ac_{ijk}^{D2} + (B - c_{ijk}^{D2})(S_{ijk}^R + S_{ijk}^B + S_{ijk}^A + \gamma B_{ijk} + \kappa F_{ijk}) - (C + c_{ijk}^{D2})\lambda G_{ijk}. \tag{17}$$

Complex cells at disparity D_2 receive both FCS excitation F_{ijk} and inhibition G_{ijk}, where λ is the disparity competition factor. The surface representation inhibitory signal (λG_{ijk}) depends upon the depth arrangement assumed for the particular stimulus. For simplicity, an explicit stage of filling-in and contour detection was not employed. Instead, as noted above, contours obtained by simple cells were taken as feedback signals. For the simulation of white horizontal lines in front,

$$G_{ijk} = S_{ijk}^A, \tag{18}$$

and for the simulation where the squares are seen in front,

$$G_{ijk} = S_{ijk}^R + S_{ijk}^B. \tag{19}$$

Equations (12) and (17) were assumed to reach equilibrium fast so that the equilibrium solutions were used. Initially, both excitatory and inhibitory FCS and CC loop signals are zero. The complex cell activities are determined by feedforward simple cell signals. These complex cell signals are used as inputs for the grouping mechanisms of the CC loop. Once the CC loop activities are determined, both CC loop and surface feedback signals provide non-zero inputs to Equations (12) and (17). The parameters are $A = 0.1$, $B = 60.0$, $C = 60.0$, $\gamma = 0.05$, $\kappa = 5.0$, and $\lambda = 4.0$.

Cooperative-Competitive Loop

Bipole cell activities are obtained in a two-pass implementation that simplifies for the

more complete recurrent implementation in, say, Grossberg, Mingolla, and Williamson (1995). The basic idea is that the first stage registers activities mid-way between the inducers. Given these initial signals, *all* remaining positions between the inducers will be able to fire in the second stage.

Stage 1. Initially, left- and right-lobe activities are computed:

$$L^1_{ijk} = \left[\sum_{pq} (c_{pqk} - c_{pqK}) F^L_{pqijk} \right]^+ \tag{20}$$

and

$$R^1_{ijk} = \left[\sum_{pq} (c_{pqk} - c_{pqK}) F^R_{pqijk} \right]^+ \tag{21}$$

where the signals F^L_{pqijk} and F^R_{pqijk} are given by oriented elongated Gaussians with the respective spatial offsets for the left and right branches. More precisely, for the horizontally oriented bipoles

$$F^L_{pqijk} = G_{pq,i-d,jk} \tag{22}$$

and

$$F^R_{pqijk} = G_{pq,i+d,jk} \tag{23}$$

where d is a spatial offset that centers the Gaussians at positions $i - d$ and $i + d$, respectively. The Gaussian G is given by equation (6). As before, left and right branches of four orientations were employed: vertical, horizontal, and two 45 degree obliques ($k = 0, 3, 6, 9$ in equation (6)). The spatial offsets thus create the two branches of the bipole kernel such that it samples signals to the left and right of position (i, j). The inhibitory complex cell input ($-c_{pqK}$), where K is the orientation orthogonal to k, implements spatial impenetrability. The bipole property is realized by gating of left-lobe and right-lobe activities, as in

$$H_{ijk} = L^1_{ijk} \times R^1_{ijk}. \tag{24}$$

The gated signals are input to a stage of on-center off-surround shunting interaction to spatially sharpen H_{ijk} signals. The output of this interaction is given at equilibrium by

$$V_{ijk} = \left[\frac{\beta C_{ijk} - \gamma D_{ijk}}{\alpha + C_{ijk} + D_{ijk}} \right]^+ , \tag{25}$$

where

$$C_{ijk} = \sum_{pq} H_{pqk} A_{pqij} \quad \text{and} \quad D_{ijk} = \sum_{pq} H_{pqk} B_{pqij}, \tag{26}$$

and A_{pqij} and B_{pqij} are Gaussian weighting functions, as in equations (3) and (4).

Stage 2. Again, left and right lobes are used:

$$L^2_{ijk} = \left[\sum_{pq} (V_{pqk} - V_{pqK}) F^L_{pqijk} \right]^+ \tag{27}$$

and

$$R_{ijk}^2 = \left[\sum_{pq} (V_{pqk} - V_{pqK}) F_{pqijk}^R \right]^+ \tag{28}$$

where the kernels F_{pqijk}^L and F_{pqijk}^R are defined as in (22) and (23). Spatial impenetrability is implemented here by terms $(-V_{pqK})$.

The final bipole activity is given by

$$B_{ijk} = \begin{cases} L_{ijk}^1 + R_{ijk}^1 & \text{if } (L_{ijk}^1 + L_{ijk}^2) > 0 \text{ and } (R_{ijk}^1 + R_{ijk}^2) > 0 \\ 0 & \text{otherwise.} \end{cases} \tag{29}$$

In other words, if there is left-lobe activity (either from the first pass or the second pass) *and* right-lobe activity (again, from either the first or second pass), then the boundary is completed at that position. Terms B_{ijk} compute an analog boundary representation that is based on the initial Stage 1 activities, which are sensitive to image contrast.

The output of the CC loop is fed back to the complex cell stage via equation (12). In practice, the CC loop is run twice. The first time it takes into account the feedforward simple cell signals and produces groupings that will determine surface filling-in (the latter was not implemented). The second time it takes into account the surface feedback to complex cells and produces groupings that are consistent with the depth representation. These final groupings determine the strength of perceived segregation. The parameters are $\alpha = 0.1$, $\beta = 4.0$, and $\gamma = 4.0$.

Strength of Perceived Segregation

The segregation scores reported in Table 1 apply to displays that explicitly contain depth (through disparity) as well as displays that do not. In order to be able to compare such scores we combine the boundary activations of the two planes (when present) to produce a final scalar value that correlates with perceived segregation.

Accordingly, for each of the two depth planes (d) employed, and for each orientation (k), we compute a *discriminability measure* dependent on the normalized differences between the final complex cell activities for the top and bottom regions of each pattern. Formally,

$$D_k^{(d)} = \frac{\left| \sum_{pq} (c_{pqk}^{(t,d)} - c_{pqk}^{(b,d)}) \right|}{\left| \sum_{pq} (c_{pqk}^{(t,d)} + c_{pqk}^{(b,d)}) \right|} \tag{30}$$

where t and b denote the top and bottom regions of the display, respectively. Note that the signals c_{pqk}, defined in (12) and (17), are the final complex cell activations taking into account surface feedback.

In order to combine different discriminabilities across depths, we first compute an *energy* measure of the complex cell activations associated with each depth and orientation. Thus

$$E_k^{(d)} = \sum_{pq} (c_{pqk}^{(t,d)} + c_{pqk}^{(b,d)}) \tag{31}$$

Finally, a scalar segregation score is obtained by

$$M = \sum_{d,k} D_k^{(d)} \left(\frac{E_k^{(d)}}{\epsilon + \sum_w E_k^{(w)}} \right) \tag{32}$$

where $\epsilon = 100.0$. In other words, the discriminability of a given depth and orientation is weighed by its associated energy with respect to the total energy (including the two depths when present) for that orientation before contributing to the overall segregation score. These final scores are the ones reported in Table 1.

Reference

Arrington, K.F. (1994). The temporal dynamics of brightness filling–in. *Vision Research*, **34**, 3371–3387.

Beck, J. (1994). Interference in the perceived segregation of equal-luminance element-arrangement texture patterns. *Perception and Psychophysics*, **56**, 424–430.

Beck, J., Graham, N., and Sutter, A. (1991). Lightness differences and the perceived segregation of regions and populations. *Perception and Psychophysics*, **49**, 257–269.

Beck, J., Prazdny, K., and Rosenfeld, A. (1983). A theory of textural segmentation. In J. Beck, B. Hope, and A. Rosenfeld (Eds.), *Human and machine vision*, pp. 1–38. New York, Academic Press.

Beck, J., Rosenfeld, A., and Ivry, R. (1989). Line segregation. *Spatial Vision*, **4**, 75–101.

Beck, J., Sutter, A., and Ivry, R. (1987). Spatial frequency channels and perceptual grouping in texture segregation. *Computer Vision, Graphics, and Image Processing*, **37**, 299–325.

Bergen, J., and Landy, M. (1991). Computational modeling of visual texture segregation. In Landy, M. and Movshon, J. (Eds.), *Computational models of visual processing*. Cambridge, Mass.: MIT Press.

Blake, A., and Zisserman, A. (1987). *Visual reconstruction*. Cambridge, MA: MIT Press.

Boynton, R. and Kaiser, P. (1968). Vision: The additivity law made to work for heterochromatic photometry with bipartite fields. *Science*, **161**, 366–368.

Bregman, A.L. (1981). Asking the "what for" question in auditory perception. In M. Kubovy and J.R. Pomerantz (Eds.), **Perceptual organization**. Hillsdale, NJ: Erlbaum Associates, 99–118.

Cohen, M., and Grossberg, S. (1984). Neural dynamics of brightness perception: Features, boundaries, diffusion, and resonance. *Perception and Psychophysics*, **36**, 428–456.

Daugman, J. (1988). Complete discrete 2-D Gabor transforms by neural networks for image analysis and compression. *IEEE Transactions on Acoustics, Speech, and Signal Processing*, **36**, 1169–1179.

DeYoe, E.A. and van Essen, D.C. (1988). Concurrent processing streams in monkey visual cortex. *Trends in Neurosciences*, **11**, 219–226.

Ferster, D. (1988). Spatially opponent excitation and inhibition in simple cells of the cat visual cortex. *Journal of Neuroscience*, **8**, 1172–1180.

Francis, G. and Grossberg, S. (1996a). Cortical dynamics of form and motion integration: Persistence, apparent motion, and illusory contours. *Vision Research*, **36**, 149–173.

Francis, G. and Grossberg, S. (1996b). Cortical dynamics of boundary segmentation and reset: Persistence, afterimages, and residual traces. Technical Report CAS/CNS-TR-95-002, Boston, MA: Boston University. *Perception*, in press.

Francis, G., Grossberg, S., and Mingolla, E. (1994). Cortical dynamics of feature binding and reset: Control of visual persistence. *Vision Research*, **34**, 1089–1104.

Gibson, J.J. (1950). **Perception of the visual world**. Boston, MA: Houghton Mifflin.

Gillam, B. and Borsting, E. (1988). The role of monocular regions in stereoscopic displays. *Perception*, **17**, 603–608.

Gove, A., Grossberg, S., and Mingolla, E. (1995). Brightness perception, illusory contours, and corticogeniculate feedback. *Visual Neuroscience*, **12**, 1027–1052.

Gouras, P. and Kruger, J. (1979). Responses of cells in foveal visual cortex of the monkey to pure color contrast. *Journal of Neurophysiology*, **42**, 850–860.

Gregory, R.L. and Heard, P. (1979). Border locking and the café wall illusion. *Perception*, **8**, 365–380.

Graham, N., Beck, J., and Sutter, A. (1992). Nonlinear processes in spatial-frequency channel models of perceived texture segregation: Effects of sign and amount of contrast. *Vision Research*, **32**, 719–743.

Griffiths, A.F. and Chubb, C. (1993). Integration of information a cross spatial frequency channels in detection of contrast boundaries. *Investigative Ophthalmology and Visual Science*, **34**, 1289.

Grossberg, S. (1983). The quantized geometry of visual space: The coherent computation of depth, form and lightness. *Behavioral and Brain Sciences*, **6**, 625–692.

Grossberg, S. (1987a). Cortical dynamics of three-dimensional form, color, and brightness perception, I: Monocular theory, *Perception and Psychophysics*, **41**, 87–116.

Grossberg, S. (1987b). Cortical dynamics of three-dimensional form, color, and brightness perception, II: Binocular theory, *Perception and Psychophysics*, **41**, 117–158.

Grossberg, S. (1994). 3-D vision and figure-ground separation by visual cortex. *Perception and Psychophysics*, **55**, 48–120.

Grossberg, S. (1997). Cortical dynamics of 3-D figure-ground perception of 2-D pictures. *Psychological Review*, in press.

Grossberg, S. and Marshall, J. (1989). Stereo boundary fusion by cortical complex cells: A system of maps, filters, and feedback networks for multiplexing distributed data. *Neural Networks*, **2**, 29–51.

Grossberg, S. and McLoughlin, N. (1997). Cortical dynamics of 3-D surface perception: Binocular and and half-occluded scenic images. *Neural Networks*, in press.

Grossberg, S., and Mingolla, E. (1985a). Neural dynamics of form perception: Boundary completion, illusory figures, and neon color spreading. *Psychological Review*, **92**, 173–211.

Grossberg, S., and Mingolla, E. (1985b). Neural dynamics of perceptual grouping: Textures, boundaries, and emergent features. *Perception and Psychophysics*, **38**, 141–171.

Grossberg, S., and Mingolla, E. (1987). Neural dynamics of surface perception: Boundary webs, illuminants, and shape-from-shading. *Computer Vision, Graphics, and Image Processing*, **37**, 116–165.

Grossberg, S., Mingolla, E., and Ross, W.D. (1997). Visual brain and visual perception: How does the cortex do perceptual grouping? *Trends in Neurosciences*, **20**, 106–111.

Grossberg, S., Mingolla, E., and Todorović, D. (1989). A neural network architecture for preattentive vision. *IEEE Transactions on Biomedical Engineering*, **36**, 65–84.

Grossberg, S., Mingolla, E., and Williamson, J. (1995). Synthetic aperture radar processing by a multiple scale neural system for boundary and surface representation. *Neural Networks*, **8**, 1005–1028.

Grossberg, S., and Todorović, D. (1988). Neural dynamics of 1-D and 2-D brightness perception: A unified model of classical and recent phenomena. *Perception and Psychophysics*, **43**, 241–277.

Grossberg, S., and Wyse, L. (1991). Figure-ground segregation of connected scenic figures: Boundaries, filling-in, and opponent processing. *Neural Networks*, **4**, 732–742.

He, Z. and Nakayama, K. (1994). Perceiving textures: Beyond filtering. *Vision Research*, **34**, 151–162.

Hubel, D. and Wiesel, T. (1968). Receptive fields and functional architecture of monkey striate cortex. *Journal of Neurophysiology*, **28**, 1041–1059.

Hubel, D.H. and Wiesel, T.N. (1977). Functional architecture of macaque monkey visual cortex. *Proceedings of the Royal Society of London (B)*, **198**, 1–59.

Jameson, D. and Hurvich, L.M. (1955). Some quantitative aspects of an opponent-colors theory: I. Chromatic responses and spectral saturation. *Journal of the Optical Society of America*, **45**, 546–552.

Julesz, B. and Krose, B. (1988). Features and spatial filters. *Nature*, **333**, 302–303.

Kanizsa, G. (1979). **Organization in vision: Essays in Gestalt perception**. New York: Praeger Press.

Kawabata, N. (1984). Perception at the blind spot and similarity grouping. *Perception and Psychophysics*, **36**, 151–158.

Kaye, M. (1978). Stereopsis without binocular correlation. *Vision Research*, **18**, 1013–1022.

Klein, S. and Stromeyer, C.F. III (1980). On inhibition between spatial frequency channels: Adaptation to complex gratings. *Vision Research*, **20**, 459–466.

Kulikowski, J.J. (1978). Limit of single vision in stereopsis depends on contour sharpness. *Nature*, **275**, 126–127.

Lawson, R.B. and Gulick, W.L. (1967). Stereopsis and anomalous contour. *Vision Research*, **1**, 271–297.

Lesher, G.W. and Mingolla, E. (1993). The role of edges and line-ends in illusory contour formation. *Vision Research*, **33**, 2253–2270.

Liu, Z., Gaska, J.P., Jacobson, L.D., and Pollen, D.A. (1992). Interneuronal interaction between members of quadrature phase and anti-phase pairs in the cat's visual cortex. *Vision Research*, **32**, 1193–1198.

Livingstone, M. and Hubel, D. (1984). Anatomy and physiology of a color system in the primate visual cortex. *Journal of Neuroscience*, **4**, 309–356.

Livingstone, M.S. and Hubel, D.H. (1987). Psychophysical evidence for separate channels for the perception of form, color, movement, and depth. *Journal of Neuroscience*, **7**, 3416–3468.

Malik, J. and Perona, P. (1990). Preattentive texture discrimination with early vision mechanisms. *Journal of the Optical Society of America A*, **2**, 923–932.

McLoughlin, N. and Grossberg, S. (1997). Cortical computation of stereo disparity. *Vision Research*, in press.

Michael, C. (1978a). Color vision mechanisms in monkey striate cortex: simple cells with dual opponent-color receptive fields. *Journal of Neurophysiology*, **41**, 1233–1249.

Michael, C. (1978b). Color-sensitive complex cells in monkey striate cortex. *Journal of Neurophysiology*, **41**, 1250–1266.

Michael, C. (1979). Color-sensitive hypercomplex cells in monkey striate cortex. *Journal of Neurophysiology*, **42**, 726–744.

Michael, C. (1981). Columnar organization of color cells in monkey's striate cortex. *Journal of Neurophysiology*, **46**, 587–604.

Michael, C. (1985). Laminar segregation of color cells in the monkey's striate cortex. *Vision Research*, **25**, 415–234.

Nakayama, K. and Shimojo, S. (1990). DaVinci stereopsis: Depth and subjective occluding contours from unpaired image points. *Vision Research*, **30**, 1811–1825.

Nakayama, K., Shimojo, S., and Ramachandran, V.S. (1990). Transparency: Relation to depth, subjective contours, luminance, and neon color spreading. *Perception*, **19**, 497–513.

Neumann, H. (1996). Mechanisms of neural architecture for visual contrast and brightness perception. *Neural Networks*, **9**, 921–936.

Ohzawa, I., DeAngelis, G.C., and Freeman, R.D. (1990). Stereoscopic depth discrimination in the visual cortex: Neurons ideally suited as disparity detectors. *Science*, **249**, 1037–1041.

Paradiso, M., and Nakayama, K. (1991). Brightness perception and filling-in. *Vision Research*, **31**, 1221–1236.

Pessoa, L. and Beck, J. (1995). Unpublished results.

Pessoa, L., Beck, J., & Mingolla, E. (1996). Perceived texture segregation in chromatic element-arrangement patterns: High luminance interference. *Vision Research*, **36**, 1745–1761.

Pessoa, L., Mingolla, E., and Neumann, H. (1995). A contrast– and luminance–driven multiscale network model of brightness perception. *Vision Research*, **35**, 2201–2223.

Peterhans, E. and von der Heydt, R. (1989). Mechanisms of contour perception in monkey visual cortex, II: Contours bridging gaps. *The Journal of Neuroscience*, **9**, 1749–1763.

Petry, S. and Meyer, G. (Eds.)(1987). **The perception of illusory contours**. New York, NY: Springer-Verlag.

Quinn, P.C. (1985). Suprathreshold contrast perception as a function of spatial frequency. *Perception and Psychophysics*, **38**, 408–414.

Richards, W. and Kaye, M.G. (1974). Local versus global stereopsis: Two mechanisms. *Vision Research*, **14**, 1345–1347.

Sagi, D. and Hochstein, S. (1984). The contrast dependence of spatial frequency channel interactions. *Vision Research*, **24**, 1357–1365.

Schiller, P.H. (1992). The ON and OFF channels of the visual system. *Trends in Neurosciences*, **15**, 86–92.

Schiller, P.H. (1995). Effect of lesions in visual cortical area V4 on the recognition of transformed objects. *Nature*, **376**, 342–344.

Schor, C.M. and Tyler, C.W. (1981). Spatio-temporal properties of Panum's fusional area. *Vision Research*, **21**, 683–692.

Schor, C.M. and Wood, I. (1983). Disparity range for local stereopsis as a function of luminance spatial frequency. *Vision Research*, **23**, 1649–1654.

Schor, C.M., Wood, I., and Ogawa, J. (1984). Binocular sensory fusion is limited by spatial resolution. *Vision Research*, **24**, 661–665.

Shipley, T.F. and Kellman, P.J. (1992). Strength of visual interpolation depends on the ratio of physically specified to total edge length. *Perception and Psychophysics*, **52**, 97–106.

Sutter, A., Beck, J., and Graham, N. (1989). Contrast and spatial variables in texture segregation: Testing a simple spatial-frequency channels model. *Perception and Psychophysics*, **46**, 312–332.

Thorell, L.G., DeValois, R.L., and Albrecht, D.G. (1984). Spatial mapping of monkey V1 cells with pure color and luminance stimuli. *Vision Research*, **24**, 751–769.

Ts'o, D. (1989). The functional organization and connectivity of color processing. In Lam, D. and Gilbert, C. (Eds.), *Neural mechanisms of visual processing* (pp. 87–115). Woodlands, TX.: Portfolio Publishing.

Ts'o, D. and Gilbert, C. (1988). The organization of chromatic and spatial interactions in the primate striate cortex. *The Journal of Neuroscience*, **8**, 1712–1727.

Tyler, C.W. (1975). Spatial organization of binocular disparity sensitivity. *Vision Research*, **15**, 583–590.

Tyler, C.W. (1983). Sensory processing of binocular disparity. In C.M. Schor and K.J. Cuiffreda (Eds.) **Vergence Eye Movements**, pp. 199–295. Boston: Butterworths.

Thorell, L.G., DeValois, R.L., and Albrecht, D.G. (1984). Spatial mapping of monkey V1 cells with pure color and luminance stimuli. *Vision Research*, **24**, 751–769.

von der Heydt, R., Peterhans, E. and Baumgartner, G. (1984). Illusory contours and cortical neuron responses. *Science*, **224**, 1260–1262.

Waxman, A.M., Seibert,M.C., Gove, A., Fay, D.A., Bernardon, A.M., Lazott, C., Steile, W.R., and Cunningham, R.K. (1995). Neural processing of targets in visible, multi-spectral IR and SAR imagery. *Neural Networks*, **8**, 1029–1052.

Wheatstone, C. (1838). On some remarkable, and hitherto unobserved, phenomena of binocular vision. *Philosophical Transactions of the Royal Society (London)*, **128**, 371–394.

Wilson, H.R. and Richards, W.A. (1989). Mechanisms of contour curvature discrimination. *Journal of the Optical Society of America*, **6**, 106–115.

Winer, B. (1962). *Statistical principles in experimental design.* New York: McGraw-Hill.

Zrenner, E., Abramov, I., Akita, M., Cowey, A., Livingstone, M., and Valberg, A. (1990). Color perception: Retina to cortex. In L. Spillmann and J.S. Werner (Eds.), **Visual perception: The neurophysiological foundations**. San Diego:Academic Press.